



TALLINN UNIVERSITY OF TECHNOLOGY
SCHOOL OF ENGINEERING
Department of Energy Technology

**CFD ANALYSIS OF THERMAL HYDRAULIC
PHENOMENA IN CASE OF IN-VESSEL RETENTION
STRATEGY FOR AN SMR**

**KOORIUMI TERMOHÜDRAULIKA NUMBRILINE
ANALÜÜS VÄIKESE MOODULREAKTORI SURVEANUMAS**

BACHELOR THESIS

Student: Rainer Kelk

Student code: 185700EACB

Supervisors: Marti Jeltsov, PhD
Research Scientist

Dmitri Nešumajev, PhD
Senior Research Scientist

Tallinn 2021

(On the reverse side of title page)

AUTHOR'S DECLARATION

Hereby I declare, that I have written this thesis independently.

No academic degree has been applied for based on this material. All works, major viewpoints and data of the other authors used in this thesis have been referenced.

/signed digitally/

Author: Rainer Kelk

Thesis is in accordance with terms and requirements

/signed digitally/

Supervisor: Marti Jeltsov

Accepted for defence

/signed digitally/

Chairman of theses defence commission: Oliver Järvik

Non-exclusive Licence for Publication and Reproduction of Graduation Thesis¹

I, Rainer Kelk (name of the author) (date of birth: 29/07/1997) hereby

1. grant Tallinn University of Technology (TalTech) a non-exclusive license for my thesis

CFD Analysis of Thermal Hydraulic Phenomena in Case of In-Vessel Retention Strategy for an SMR,

(title of the graduation thesis)

supervised by Marti Jeltsov,

(Supervisor's name)

1.1 reproduced for the purposes of preservation and electronic publication, incl. to be entered in the digital collection of TalTech library until expiry of the term of copyright;

1.2 published via the web of TalTech, incl. to be entered in the digital collection of TalTech library until expiry of the term of copyright.

1.3 I am aware that the author also retains the rights specified in clause 1 of this license.

2. I confirm that granting the non-exclusive license does not infringe third persons' intellectual property rights, the rights arising from the Personal Data Protection Act or rights arising from other legislation.

¹ *Non-exclusive Licence for Publication and Reproduction of Graduation Thesis is not valid during the validity period of restriction on access, except the university's right to reproduce the thesis only for preservation purposes.*

/signed digitally/

Department of Energy Technology

THESIS TASK

Student: Rainer Kelk, 185700EACB

Study programme: EACB17/17 - Keskkonna-, energia- ja keemiatehnoloogia

Main speciality: Energiatehnoloogia

Supervisors: Marti Jeltsov, Research Scientist, +37258363388

Dmitri Nešumajev, Senior Research Scientist, +3726203910

Thesis topic:

(in English) *CFD analysis of thermal hydraulic phenomena in case of In-Vessel Retention strategy for an SMR*

(in Estonian) *Kooriumi termohüdraulika numbriline analüüs väikese moodulreaktori surveanumas*

Thesis main objectives:

1. Studying the literature
2. Creating the model
3. Simulating the thermal-hydraulic core melt processes

Thesis tasks and time schedule:

| No | Task description | Deadline |
|----|---|------------|
| 1. | Studying the literature | 01/03/2021 |
| 2. | Creating the model and simulating the physics | 01/05/2021 |
| 3. | Writing the thesis | 01/06/2021 |

Language: English

Deadline for submission of thesis: June 4, 2021

Student: Rainer Kelk /signed digitally/

Supervisors: Marti Jeltsov /signed digitally/

Dmitri Nešumajev /signed digitally/

Head of study programme: Oliver Järvik /signed digitally/

Terms of thesis closed defence and/or restricted access conditions to be formulated on the reverse side

CONTENTS

| | |
|--|----|
| PREFACE | 6 |
| List of abbreviations and symbols | 7 |
| INTRODUCTION..... | 9 |
| 1. IN-VESSEL MELT RETENTION STRATEGY | 11 |
| 1.1 Thermal hydraulics of the corium pool | 12 |
| 1.1.1 Non-dimensional numbers | 12 |
| 1.1.2 Stratification process | 13 |
| 1.1.3 Oxidic layer | 14 |
| 1.1.4 Metallic layer | 18 |
| 1.2 Thermal failure of the RPV | 21 |
| 1.2.1 Critical heat flux and boiling crisis | 21 |
| 1.2.2 Structural failure of the RPV | 22 |
| 1.3 Increasing the efficiency of the IVMR strategy | 23 |
| 2. MODELLING THE CORIUM POOL..... | 24 |
| 2.1 Flow domain and geometry | 25 |
| 2.1.1 Dimensionality | 25 |
| 2.1.2 Geometry | 26 |
| 2.2 Boundary and initial conditions | 29 |
| 2.2.1 Reactor pressure vessel | 29 |
| 2.2.2 Oxidic pool | 30 |
| 2.2.3 Metallic layer | 33 |
| 2.3 Mesh generation | 34 |
| 2.4 Simulation strategy | 36 |
| 2.4.1 Validation against BALI experiment | 37 |
| 2.5 Mesh Independence Study | 41 |
| 2.5.1 Grid convergence study of the IVMR problem..... | 42 |
| 2.6 Simulation results | 43 |
| 3. CONCLUSIONS AND DISCUSSION..... | 46 |
| SUMMARY..... | 47 |
| KOKKUVÕTE | 49 |
| LIST OF REFERENCES | 51 |
| APPENDIX 1 Pikendatud kokkuvõte..... | 55 |

PREFACE

The basis for this thesis stemmed from my ever-growing interest in nuclear engineering due to its possible positive impact on the Estonian energy mix. This thesis would act as a stepping-stone to the world of computational fluid dynamics (CFD) while retaining the close connection to nuclear engineering.

The thesis topic was initiated by Marti Jeltsov, Head of the Nuclear Science and Engineering group at NICPB (National Institute of Chemical Physics and Biophysics). Thesis work was done from home due to COVID-19 limitations and the possibilities of CFD.

The research and simulation was a constant trial-and-error process as I had not worked with CFD before. The whole process was made much easier by having my two supervisors always at the ready to assist me and answer my question. I owe a great debt of gratitude to both Marti Jeltsov and Dmitri Nešumajev for guiding me through the challenging process and giving me tips along the way. I would also like to thank Elering AS for supporting the creation of this thesis and the development of energy systems of the future.

In-vessel melt retention is a very attractive strategy for severe accident mitigation as it preserves the integrity of the last containment barrier. For reactors of power below 600 MWe, the evaluated safety margins are sufficient but for small modular reactors, the evaluation is still needed due to compact nature of the SMR designs. This thesis explains the theoretical background of thermal hydraulics of the IVMR strategy, and in the second part simulates the stratified steady-state corium pool. The reference quasi-SMR for this simulation is based on BWRX-300 and BWR-5. AHFM-NRG+ turbulence model is used to simulate the turbulent flow of the domain. The results from the simulations indicate that in the steady state, structural integrity is preserved as the local heat flux stays well below the critical heat flux. However, further assessment is needed to determine the local heat flux values during transients.

IVMR, CFD, thermal hydraulics, core melt, bachelor thesis

List of abbreviations and symbols

Abbreviations

- BC – Boiling crisis
- BWR – Boiling water reactor
- CFD – Computational fluid dynamics
- CHF – Critical heat flux
- CRGT – Control rod guiding tube
- EVMR – Ex-Vessel Melt Retention
- IVMR – In-Vessel Melt Retention
- LWR – Light water reactor
- PWR – Pressurized water reactor
- RPV – Reactor pressure vessel
- SA – Severe accident
- SAM – Severe accident management
- SMR – Small Modular Reactor

Symbols

- Ra – Rayleigh number
- Gr – Grashof number
- Da – Damköhler number
- Pr – Prandtl number
- Pr_t – Turbulent Prandtl number
- g – acceleration of gravity
- β – thermal expansion co-efficient
- T – temperature
- H – characteristic length
- ν – kinematic viscosity
- α – thermal diffusivity
- C_p – specific heat

μ – dynamic viscosity
 k – thermal conductivity
 \dot{Q} – volumetric heat generation
 q – heat flux
 V – volume
 S – surface area
CF – concentration factor
 R – radius
 θ – contact angle
CHF – critical heat flux
 Q – total heat
 D – diameter
 δ – wall thickness
 P_t – power (thermal)
 ρ – density
 R_λ – thermal insulance
GCI – grid convergence index
 F_s – factor of safety
 ϵ – relative error
 r – grid refinement ratio
 p – order of convergence
 N – total number of grid points
 f – solution of the grid

INTRODUCTION

The first commercial nuclear power plant to generate electricity for a power grid, started operations in Obninsk of the Soviet Union on June 27, 1954. Since then, the world's nuclear power plant fleet has over 18,000 reactor years of experience [1]. During those 18,000 years there have been three major accidents – Three Mile Island, Chernobyl, and Fukushima - which have led to a partial or a complete meltdown of the nuclear reactor core.

A nuclear meltdown is a severe accident which occurs when the heat generated by a nuclear reactor exceeds the heat removed by the cooling systems. As the decay heat accumulates in the fuel elements and the steel chassis, they begin to melt. The molten mass – corium – relocates to the lower plenum of the reactor pressure vessel (RPV).

Regarding the severe accident management (SAM), there are two strategies to deal with the molten corium inside the RPV. One possibility, the Ex-Vessel Melt Retention (EVMR) is to let it melt through the vessel wall and to trickle down to a device called core catcher which prevents the corium further escaping the containment building. In-Vessel Melt Retention (IVMR) keeps the corium inside the vessel by cooling the vessel's lower head externally. The IVMR strategy is attractive because it prevents large masses of radioactive materials and gases escaping the pressure vessel. In the most robust form, the IVMR strategy also appears less expensive than an external core catcher.

Although the IVMR strategy is not new [2], the coming of the small modular reactors (SMRs) poses questions about implementing the strategy to those new designs. The IVMR strategy has proved to work at low and medium residual power levels but the SMRs pose a geometrical challenge. Because of the integral nature of the designs, the flow paths might be different and need to be therefore re-assessed.

The main objective on this bachelor's thesis is to describe the thermal hydraulic phenomena in the stratified corium and to evaluate the possibility of implementing the IVMR strategy to small modular reactors. A numerical study of severe accident in the nuclear reactor is presented. An axisymmetric 2D model of the lower plenum of a 300 MWe BWR reactor was used and full dryout was assumed. The numerical study was carried out with a commercial computational fluid dynamics (CFD) based simulation software called Simcenter STAR-CCM+.

The first chapter of the thesis focuses on the occurring phenomena and the basis of the IVMR strategy. The second chapter describes the modelling process with validation of the model and the mesh independence study. The numerical study also gives an approximate value of the steady-state ex-vessel heat flux which is one of the critical inputs for the feasibility of the IVMR strategy.

1. IN-VESSEL MELT RETENTION STRATEGY

The in-vessel retention of molten corium by cooling the vessel externally was first introduced nearly 30 years ago [3]. The Three Mile Island accident in 1979 had presented a scenario where it would be impossible to prevent the dryout of the nuclear core. Therefore, a solution was proposed – to submerge the lower head of the RPV under water in order to cool the molten mass of fuel and debris externally.

The concept was first applied to two types of reactors: AP600 [2] and VVER-440 in Loviisa, Finland [4]. As the VVER-400 fleet remained popular in European countries like Hungary, Slovakia, and Czechia, IVMR strategy was further implemented as part of the SAM. The AP600 was replaced by the AP1000 design. Both of these designs are versions of PWR. The first BWR to implement the IVMR strategy was SWR-1000 in 2001. [5]

The concept is still attractive nowadays as it is included in the design of some newer Gen III reactors like AP-1000 and the Chinese CPR-1000. The challenge of implementing the IVMR in the SAM is the higher power of the new designs. The feasibility of the IVMR strategy has been thoroughly proven [5] for sub 600 MWe conventional reactors but further research is needed to demonstrate the adequacy of the concept for higher power reactors.

Small modular reactors (SMRs) are by definition advanced reactors that produce electricity of up to 300 MWe. In regards of implementing the IVMR strategy, SMRs pose a challenge because of the integral and compact nature of the design which leaves less room for the external coolant in case of implementing the IVMR strategy. Most of the SMR designs have an insulation on the outer side of the RPV to enhance the thermal efficiency during the normal operation. This has the opposite effect during the external cooling – because of the insulation less heat can be removed from the corium. These two differences from the conventional reactors make the further research and development of the IVMR strategy necessary for SMR designs.

The IVMR strategy requires only two actions at the SA signal – flooding of the reactor cavity and depressurizing the reactor pressure vessel. This makes in-vessel melt retention robust and passive whereas maintaining the structural integrity of the containment and the vessel. The main difficulties of the IVMR analysis lie on corium behaviour evaluation and the correct boundary condition assumptions due to the possible formation and melting of the corium crust. [6]

1.1 Thermal hydraulics of the corium pool

During a severe accident in light water reactors (LWR), the lack of cooling agent around the fuel elements leads to core heat up and melting of the materials. The melt (corium) then relocates to the lower plenum of the RPV. The heat generating components are then in liquid form and continues to emit decay heat which needs to be cooled to maintain the structural integrity of the RPV.

1.1.1 Non-dimensional numbers

Non-dimensional numbers are used to describe the thermal hydraulic processes in the corium pool with internal heating and to compare and validate the computational results with experimental results.

The main driving forces of the corium pool are dominated by natural convection phenomena which can be characterized in terms of the non-dimensional Grashof (Gr), Prandtl (Pr) and Damköhler (Da) numbers. Experience also indicates a great dependency on the Rayleigh number. Rayleigh number represents the ratio of buoyancy and thermal diffusivity. Rayleigh number for fluids with internal heat generation (internal Rayleigh) is given as:

$$Ra_i = Gr \cdot Pr \cdot Da \quad (1.1)$$

Rayleigh number for fluids without heat generation is given as:

$$Ra = Gr \cdot Pr \quad (1.2)$$

Heat transfer due to natural convection is characterized by the Grashof number. It reflects the force acting on the fluid due to the difference in temperatures [7]. Grashof number is given as:

$$Gr = \frac{g\beta\Delta TH^3}{\nu^2} \quad (1.3)$$

where g is the gravity, β is the thermal expansion co-efficient, ΔT is the temperature difference between the surface and the bulk of the fluid, H is the characteristic length (here it is the height of the pool) and ν is the kinematic viscosity.

The Prandtl number represents the ratio of momentum diffusivity to thermal diffusivity. For fluids with large Prandtl number, the momentum diffusivity dominates. Vice versa, for fluids with low Prandtl number, the thermal diffusivity dominates. The Prandtl number is not dependent on geometry. The Prandtl number is given as:

$$\text{Pr} = \frac{\nu}{\alpha} = \frac{C_p \mu}{k} \quad (1.4)$$

where C_p is specific heat, μ is the dynamic viscosity and k is thermal conductivity of the fluid.

The Damköhler number is the ratio of reaction timescale to the convection time scale, flow rate through reactor for continuous processes. The Damköhler number is given as:

$$\text{Da} = \frac{\dot{Q}H^2}{k\Delta T} \quad (1.5)$$

where \dot{Q} is the volumetric heat generation, H is the characteristic length (here it is the height of the pool), k is the thermal conductivity and ΔT is the temperature difference between the surface and the bulk of the fluid

The Nusselt number describes the heat transfer on the boundary of a fluid and a solid body. The Nusselt number is also known as the dimensionless convective heat transfer coefficient because of the inclusion of thermal conductivity. The Nusselt number is defined as: [7]

$$\text{Nu} = \frac{qH}{k\Delta T} \quad (1.6)$$

where q is the average heat flux over a boundary, H is the characteristic dimension, k is thermal conductivity and ΔT is the temperature difference between the surface and the bulk of the fluid.

If the Nusselt number is close to one, the convection and conduction are of similar magnitude, and it represents laminar flow. A larger Nusselt number corresponds to more dominant convection with 100...1000 range representing turbulent flow. [8]

1.1.2 Stratification process

Corium consists of four major components – zirconium from the fuel cladding, steel from the integral structures, uranium from the fuel and oxygen from oxidation and the fuel. In addition to the mentioned components, fission products and transuranic elements are also present in the corium pool as they are by-products of fuel irradiation. The U-Zr-O-Fe molten pool undergoes separation between non-miscible metallic and oxide phases due to chemical reactions and density differences. [9]

After the initial corium relocation, the phase separation at equilibrium leads to the creation of heavy metal layer. At this moment, the steel structures have not yet molten

into the pool. The addition of the lighter steel from the structures leads to layers inversion. After the inversion, the metal layer keeps thickening due to partial melting of the RPV. The final steady state is pictured in Figure 1.1 (right) with the metallic layer being on top of the molten oxidic pool with the oxide crust separating the layers. [9]

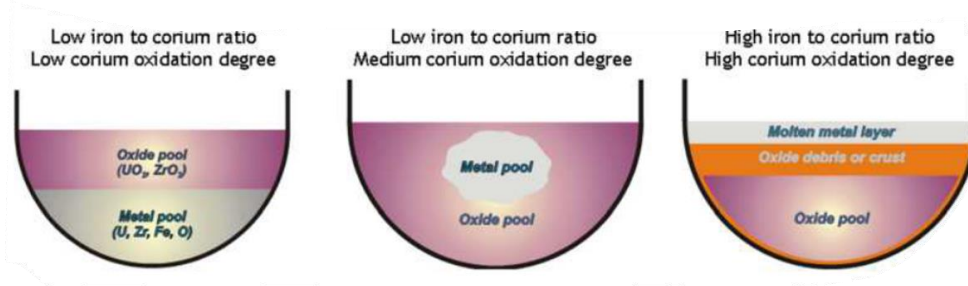


Figure 1.1: Examples of changes of corium pool configuration [5]

The parameters defining the thermodynamic equilibrium of the corium pool can be expressed in terms of: [10]

- the temperature distribution of the system;
- the Zr oxidation degree and U/Zr atomic ratio of the oxidic corium in the pool;
- the mass ratio x_{steel} between the steel and oxidic corium in the system.

The kinetics of the layers' inversion is driven by the Nusselt number, the species diffusion coefficient, and the thickness of the interaction layer. The biggest uncertainty lies in the diffusion coefficient as there is no experimental measurement available. [9]

1.1.3 Oxidic layer

The basic features of the flow regime in the oxidic layer consist of steep boundary layer regions, a well-mixed upper pool volume, and a broadly stratified lower pool portion as depicted in Figure 1.2. [2]

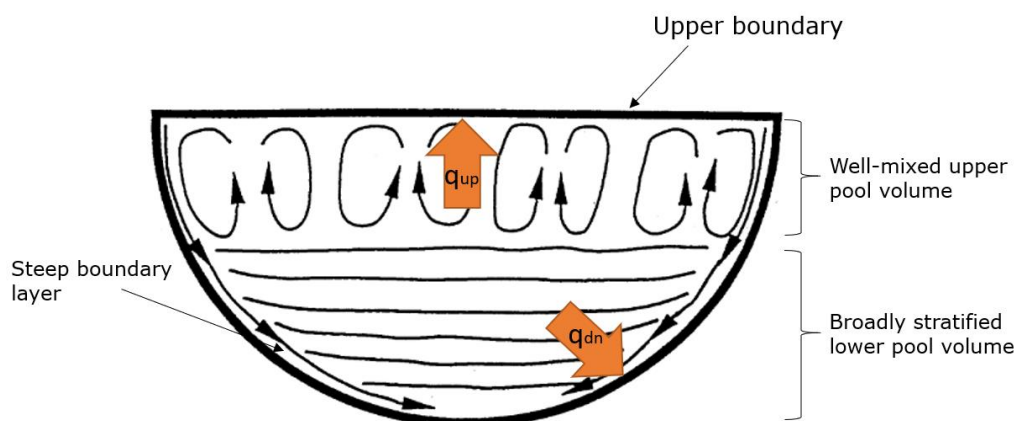


Figure 1.2: Natural convection flow and stratification in the oxidic pool [2]

The regions can be expected as they have been experimentally proven and demonstrated in experiments like BALI [11], COPO [2] and SIMECO [8]. The COPO experiments with hot water for VVER-440 reactor [2] showed that for internal Rayleigh values $10^7 < Ra_i < 6 \cdot 10^{14}$, the correlation for the upper boundary can be summarized as:

$$Nu_{up} = 0.345 \cdot Ra_i^{0.233} \quad (1.7)$$

The upward Nusselt correlation is the most important indicator as this describes the upward heat flux resulting in superheating of the metallic layer and the magnitude of the focusing effect (described in 1.1.4). Correlation (1.7) is however only one of the many correlations for global Nusselt number. For each geometry and composition case, the validity of the correlation has to be re-assessed.

The overall heat balance of the oxidic pool can be written as:

$$\dot{Q}V = S_{up}q_{up} + S_{dn}q_{dn} \quad (1.8)$$

where \dot{Q} is the volumetric heat source, V is the volume of the oxidic pool, S is the surface area of the boundary considered, and the q_{up} and q_{dn} depend on the local Nusselt number values which derive from the internal Rayleigh number values.

For BWR type reactors, the geometry differences due to a large number of CRGTs in the lower plenum (Figure 2.2) alter the flow pattern. In BWRs, the flow pattern is expected to be governed more by the local flow pattern rather than by the pool's global circulation pattern [12].

The oxide crust behaviour

Due to external cooling, solidification takes place at the periphery forming a layer of crust around the molten corium. This phenomenon is one of the keys in assessing the feasibility of the IVMR strategy. Experimental studies have identified thermal and physicochemical phenomena taking place in the corium crust and their impact on the kinetics of the pool stratification. The behaviour of corium crust is well-understood in the steady state two-layered configuration but the transient phenomena are not well researched and many modelling assumptions are made. [13]

The oxide crust reduces the thermal load to the reactor vessel acting as a thermal resistance due to the lower thermal conductivity value of the crust compared to the one of the oxidic pool. Because the melting of the oxide crust at the interface between two

layers is likely as soon as the temperature of the metallic layer exceeds the liquidus temperature of the oxide, the focusing effect is enhanced [14].

The crust characteristics and behaviour depend on its location. As discussed earlier, the crust between the metallic layer and the oxidic pool can be neglected as it is bound to melt in steady-state configuration due to significantly higher than liquidus temperatures of both metallic and oxidic layers. However, in transient cases, the horizontal crust also slows down mass transfer but the transfer of molten steel still occurs due to the formation of cracks and channels in the crust. [14]

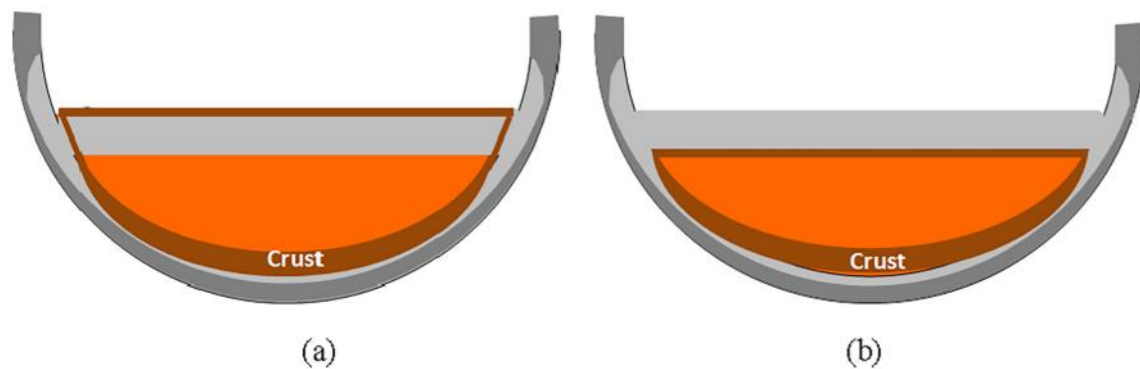


Figure 1.3: Corium configuration after stratification with the crust surrounding (a) or not (b) the top metallic layer [14]

Another uncertainty lies in the stability of the corium crust. The issue is whether, after the development of the final two-layered steady state configuration, the oxidic crust surrounds the metallic layer or not (Figure 1.3). In case of the oxidic crust being present around the metallic layer (case a), the heat flux transmitted to the vessel wall is reduced by a factor of 3 compared to the metallic layer not being surrounded by the oxidic crust (case b). [14]

Decay heat

Following the shutdown of the nuclear reactor (SCRAM), there are various nuclear species and processes that remain which are capable of generating heat (Figure 1.4). Should the cooling capability of the reactor be compromised, it may lead to a coolant boiling and eventual dry-out of the reactor core. Due to the loss of cooling agent, the heat starts to accumulate in the nuclear core, leading to a rise in temperature and consequent melting of the core. After relocation of the core, the pool of molten core continues to be internally heated.

The decay heat originates from the beta and gamma decay of fission products and transuranic elements accumulated in the nuclear fuel. Due to the unstable nature of the fission products, they undergo radioactive decays. Fission products with a short half-life are much more radioactive and contribute significantly to the decay heat at the start but because of the short half-life, the share drops rapidly. [15]

The heat generation rate is assumed to be uniformly distributed throughout the oxidic pool and the crusts, whereas some of this decay heat will escape the molten oxidic pool as gammas. Some of these gammas are deposited in the vessel wall or the metallic layer and some will escape the system. Sensitivity calculations have indicated that such effects are negligible. [2]

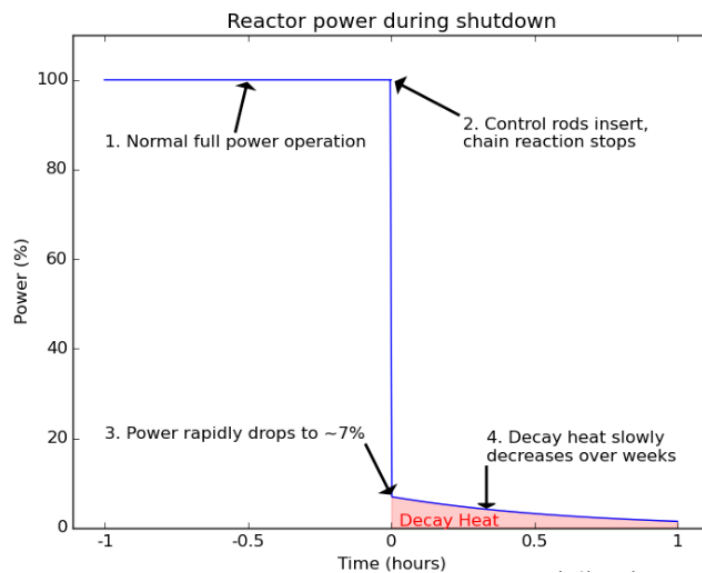


Figure 1.4: Relative power of a nuclear reactor before and after shutdown [16]

For the volumetric heat generation rate, the volume of the oxidic pool and the timing for the formation of the configuration have to be considered. To preserve the conservativity of the calculations, earliest state shall be considered. Since the material relocation to the lower head requires core melting with significant structural melting, the most probable timing for the AP-600 reactor was found to be 4+ hours which would represent decay heat being $\sim 0.5\%$ of the nominal power. [2].

The decay heat rates also depend on the fuel used in the reactor. The PWR and BWR decay rates are similar but using MOX fuel results in higher specific decay heat rate than UOX. For this thesis, UOX fuel is considered. [17]

1.1.4 Metallic layer

The heat transfer process in the metallic layer is divided into two parts – heat transfer through natural convection, as Rayleigh-Benard convection without sidewall cooling and heat transfer to the vertical interface, which is cooled by ambient air above the metallic layer. For the correlations, case a (Figure 1.3) is considered.

For the Rayleigh-Benard convection, the Globe and Dropkin correlation [18] is used:

$$Nu = 0.069Ra^{1/3}Pr^{0.074} \quad (1.9)$$

For the vertical heat transfer, the Churchill and Chu correlation [19] can be used:

$$\sqrt{Nu} = 0.825 + \frac{0.387Ra^{1/6}}{\left[1 + \left(\frac{0.492}{Pr}\right)^{9/16}\right]^{8/27}} \quad (1.10)$$

The components of the metallic layer are Fe and Zr. It is assumed that all of the decay heat originates from the oxidic pool. Illustration of the energy paths in the metallic layer is shown in Figure 1.5.

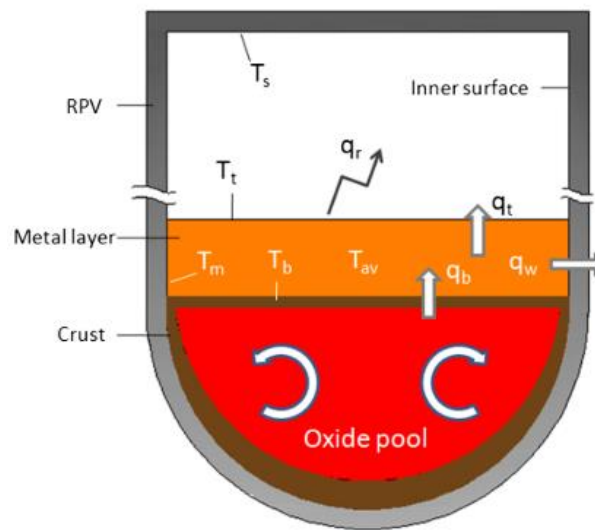


Figure 1.5: Energy paths in the metallic layer [20]

The decay heat from the oxidic pool q_b is transferred from the oxidic pool to the metallic layer through the oxide crust. The heat is then divided into two parts - q_w is transferred directly to the RPV wall through thermal conduction and the other part q_t is transferred to the surrounding RPV internal surfaces through thermal radiation. Therefore, the complete energy balance can be given as:

$$S_b q_b = S_w q_w + S_t q_t \quad (1.11)$$

The bottom heat flux q_b depends on the energy split of the oxidic layer which in turn highly depends on the flow patterns and decay heat of the oxidic pool.

Focusing effect

Focusing effect characterizes the amplification of heat flux on the RPV wall. To evaluate the focusing effect, the concentration factor (CF) is used. The concentration factor is defined as the ratio of the horizontal wall flux and bottom heat flux:

$$CF = \frac{q_w}{q_b} \quad (1.12)$$

If the top surface of the metallic layer is considered adiabatic and the thermal radiation flux is neglected ($q_t = 0$), the problem becomes more conservative, and the concentration factor can be given as:

$$CF = \frac{q_w}{q_b} = \frac{S_b}{S_w} = \frac{\pi R^2}{2\pi R H} = \frac{R}{2H} \quad (1.13)$$

where R is the inner radius of the RPV, and H is the height of the metallic layer. This equation illustrates the impact of the height of the metallic layer – the lower the height of the metallic layer, the more severe the focusing effect.

In case of the IVMR strategy with real reactor conditions, the outside surface of the RPV is considered to be isothermal, while the temperature of the metallic layer upper surface depends on the thickness of the layer and the heat flux transferred from the oxide layer. Wang and Cheng [20] illustrated the effect of the ratio H/R on the concentration factor (Figure 1.6). They considered 5 cases – realistic boundary conditions with different bottom surface heat fluxes (coloured nodes), neglecting the radiative heat flux (black line) and with cooling of the metal layer from the top by water injection (dotted line).

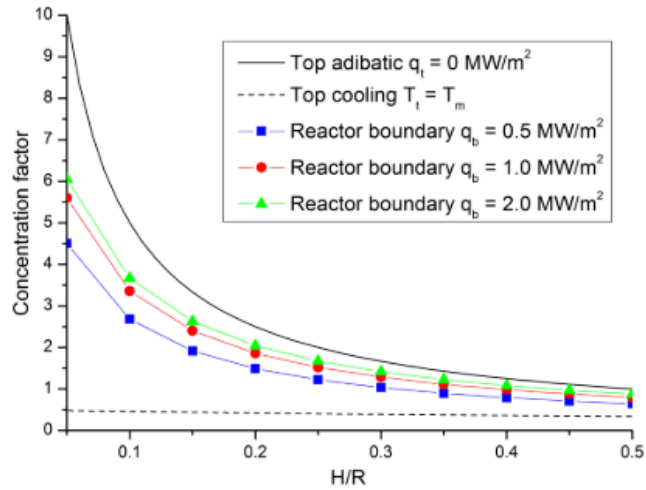


Figure 1.6: Concentration factor at different boundary conditions [20]

From the Figure 1.6, it can be seen that the concentration factor decreases with the increase of the ratio H/R . This means that the horizontal wall heat flux increases with decreasing of the metal layer height. The figure also illustrates the effect of top surface cooling as the concentration factor value remains very low.

Due to the effect of the metal layer height on the focusing effect, the transient stratification phases are the most dangerous regarding the thermal failure of the RPV. With the configuration changing from left to right (Figure 1.1), the top metal layer would be quite thin at first, as the three-layered (metallic-oxidic-metallic) configuration is formed. This causes amplified focusing effect, which in turn causes higher lateral heat fluxes.

1.2 Thermal failure of the RPV

In case of a severe accident, the reactor pressure vessel is depressurized and the dead-weight loads do not play a significant role in structural failure mechanism – thermal stresses and creep are to be mainly considered instead. [2]

1.2.1 Critical heat flux and boiling crisis

The most limiting thermal failure mechanism of the lower head is the boiling crisis (BC). Boiling crisis is defined as a state when the nucleate boiling shifts to film boiling due to a thin film of vapor blanketing the wall. Film boiling is characterized by considerably lower heat transfer coefficients. As seen in Figure 1.7, the heat flux which corresponds to the critical point and the boiling crisis, is called critical heat flux (CHF). [21]

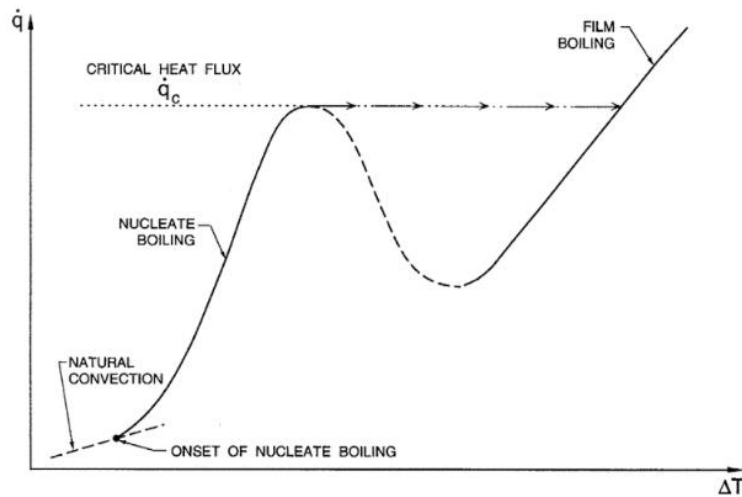


Figure 1.7: Pool boiling characteristics [21]

The determining factor of the CHF is the temperature difference ΔT of the saturation temperature of the fluid and the surface. Because the boiling process depends on both surface inclination and scale, the CHF is at its maximum at lateral heat exchange processes which describes the mechanisms present at the focusing effect phenomenon. This is caused by the rising vapor giving rise to the vapor bubbles near the equator of the lower head hemisphere which minimizes the vapor squeeze effect. [2]

The analytical equation of critical heat flux for water as a function of contact angle in degrees (θ) and degree of subcooling (ΔT_{sub}) is given by Theofanous et al [2] as:

$$\text{CHF} = 0.4(1 + 0.021\theta - (0.007\theta)^2)(1 + 0.036\Delta T_{sub}) \quad (1.14)$$

The degree of subcooling is defined as the difference between saturation temperature of liquid and actual temperature of liquid. The degree of subcooling is modified by the

complex boiling and mixing patterns outside the RPV which is not the scope of this thesis. However, (1.14) shows the impact of effective cooling and mixing of the recirculating cooling agent.

More robust way of approximately evaluating the critical heat flux for IVMR strategy as a function of only the contact angle in degrees is given as:

$$\text{CHF} = 490 + 30.2\theta - 8.88 \cdot 10^{-1}\theta^2 + 1.35 \cdot 10^{-2}\theta^3 - 6.65 \cdot 10^{-5}\theta^4 \quad (1.15)$$

1.2.2 Structural failure of the RPV

Structural failure of the RPV is highly unlikely unless there is a boiling crisis. Therefore, thermal failure is the presumption for structural failure and the only possible cause for its occurrence regarding the IVMR strategy.

Theofanous et al [2] demonstrated that a CHF-limited wall thickness is sufficient to support the lower head and the corium. The critical region of the focusing effect is around $\theta = 90^\circ$ (Figure 1.8) which is also the area with the highest possible CHF.

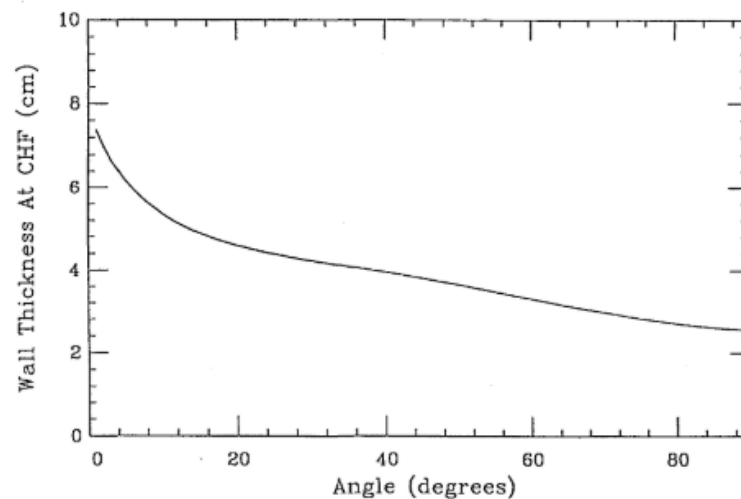


Figure 1.8: Minimum wall thicknesses required to accommodate the CHF [2]

As deadweight and buoyancy nearly cancel each other out, these factors do not play a role in the structural failure of the RPV. Thermal stress analysis also confirms that structural failure margins are larger than margins to boiling crisis which means that BC is a conservatively limiting structural failure criterion. [2]

1.3 Increasing the efficiency of the IVMR strategy

Even though the IVMR strategy is quite robust, it could be further improved by engineering practices suggested by Fichot et al [22]. Implementation of these innovations would need extensive research and development between industrial and research partners. This bachelor thesis studies the potential of the IVMR strategy for SMRs.

Increasing the mass of steel

By increasing the total mass of steel in the corium, the maximum heat flux to the vessel would decrease due to thickening of the metallic layer and lowering the focusing effect. This could be implemented by installing steel structures in the RPV to add more mass of steel during the relocation. The increased amount of steel would also remove heat through melting.

In-vessel injection

The probability of occurrence of transients leading to an early core melt could be decreased by implementing in-vessel injection. Before core-melting, the injection would delay the complete melting and after core relocation, it would cover the top metal layer and prevent the focusing effect being present. Figure 1.6 (dotted line) also demonstrates the effect of top cooling on the value concentration factor and the focusing effect. In-vessel injection would also enhance Zr oxidation impacting the corium stratification towards two-layered configuration.

External coating of the vessel

Spraying the RPV externally would improve the outside cooling based on existing small-scale experiments. By coating the vessel, higher CHF values have been obtained which could contain or slow down release of molten core solution. By "cold spray" coating, UJV Group has demonstrated CHF value improvements up to 25%. These test, however, were small scale and large-scale experimentation is needed to confirm the results.

Improving the external vessel cooling

To improve the external cooling of the vessel during transient phases with higher decay heat, forced circulation could be used together with natural circulation. Spray cooling could also be introduced to cool the RPV until the injected water reaches its intended height.

2. MODELLING THE CORIUM POOL

The second part of the thesis describes the modelling process of the corium pool and the lower head of the RPV. The whole process can be divided into 10 steps.

Table 2.1: CFD analysis process [23]

| Number | Step description |
|---------------|---|
| 1 | Formulating the flow problem |
| 2 | Modelling the geometry and flow domain |
| 3 | Establishing the boundary and initial conditions |
| 4 | Generating the grid (mesh) |
| 5 | Establishing the simulation strategy |
| 6 | Establishing the input parameters and files |
| 7 | Performing and monitoring the simulation |
| 8 | Post-processing the simulation to get the results |
| 9 | Repeating the process to examine sensitivities |
| 10 | Documenting |

According to those steps, the second part of the thesis is divided into sub-paragraphs to explicitly specify the choices made and the reasoning behind them.

The simulation is carried out in a commercial software by Siemens Digital Industries Software called Simcenter STAR-CCM+. It is a multiphysics CFD software for modelling and simulation of a wide range of physics and flow processes. The integrated environment includes CAD, automated meshing, multiphysics CFD and sophisticated postprocessing [24]. STAR-CCM+ was first developed by CD-adapco under the name of STAR-CD which was founded in 1980 in Imperial College London. The lead academics behind the birth of the software were David Gosman and Raad Issa. The company and the software were bought out by Siemens in 2016. [25]

2.1 Flow domain and geometry

This sub-paragraph encompasses steps 1-2 of the CFD analysis process (Table 2.1). The first task is to define the objective and the geometrical conditions of the analysis.

The objective of the analysis is to model the natural convection in a two-layered corium pool, whereas the lower oxide layer has a volumetric heat source simulating the decay heat. This analysis would be describing the steady state of the turbulent flow in a cavity.

2.1.1 Dimensionality

Several core-melt experiments and simulations have been performed in 2D or 3D pool geometries. In real life, the process of course takes place in a three-dimensional environment but for the simulation, 3D is computationally much more demanding. To assess the effectiveness of 2D models in capturing different flow patterns and heat exchange, thorough research has been carried out.

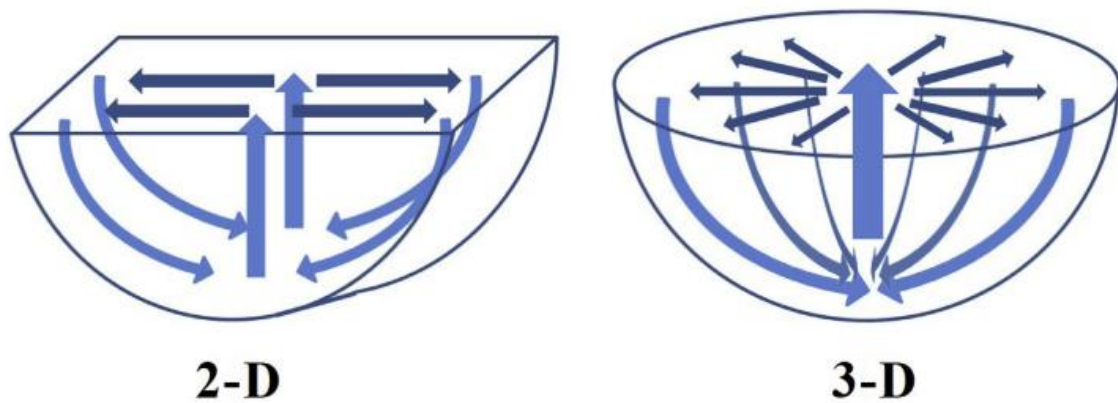


Figure 2.1: Difference of flow patterns between 2D and 3D geometries [26]

Considering the geometry of a BWR design, axisymmetric 2D domain would not simulate the effects of the continuously cooled control rod guiding tubes (CRGTs). As observed by Torregrosa et al. [27], the structural creep of the RPV wall starts to accelerate ~15 minutes later in the 3D model than in the 2D model which did not consider the CRGT cooling.

Kim, Park and Chung [26] observed different flow patterns for 2D and 3D geometries (Figure 2.1) in the oxide pool. In a 2D geometry, the flows move on a plane, whereas the 3D geometry displays radial dispersion of the upward flows and are therefore expected to be weakened as they proceed to the edges. Since the 2D flows move linearly, they are not significantly weakened, which leads to more uniform and higher upward heat transfer.

After performing 3D IVR natural convection experiments simulating the oxide layer and comparing the results with the 2D experiments, Bae and Chung [28] observed that the influence of the main-flow on the top plate heat transfer was larger for the 3D experiments than for the 2D experiments. Also, the heat dispersion in the domain was monitored. The Q_{up}/Q_{tot} ratio, which describes the focusing effect, was lower for the 3D case. This indicates that the heat dispersion in the 3D geometry is larger than in the 2D domain and therefore the focusing effect is also less severe in the 3D geometry.

Filippov and Kamenskay [29] stated that the estimated mesh size for correct modelling of the stratified melt pool was close to 100M cells but to accelerate calculations, 2D axisymmetric approach may be used as they showed satisfactory results in cases of moderate Rayleigh numbers ($Ra_i \leq 10^{14}$).

Considering the findings of the mentioned papers and the steady-state condition of the flow problem, 2D axisymmetric is the better choice because of the computational efficiency and the more conservative nature of the simulation which is described by the higher heat transfer to the molten metal pool above the oxide layer.

2.1.2 Geometry

The RPV geometry used in the quasi-SMR simulation is based on the GE-Hitachi's BWRX-300 small modular reactor (Figure 2.2). BWRX-300 is a 300 MWe water-cooled, natural circulation SMR. BWRX-300 is the tenth generation of the GE's BWR family. The BWRX-300 plant goal is to have a 95% capacity factor. [30]

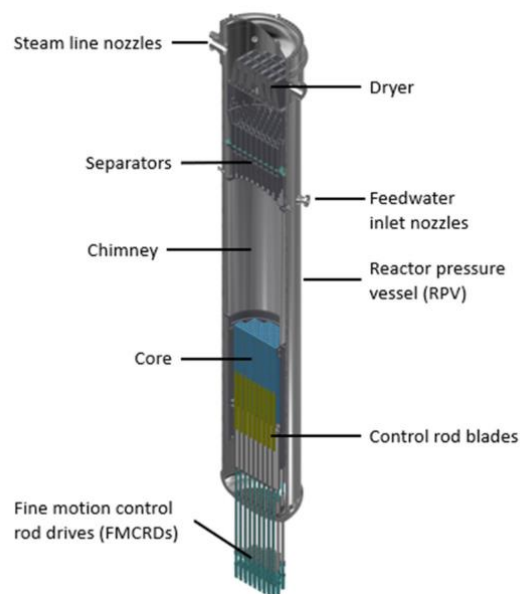


Figure 2.2: BWRX-300 reactor pressure vessel with internals [30]

The measurements of the RPV were obtained from the General Description of the BWRX-300. The key parameters of the pressure vessel are listed in Table 2.2.

Table 2.2: Key parameters of the RPV

| | |
|--|---------|
| Inside diameter D | 4 m |
| Wall thickness δ | 0.136 m |
| Total height H_{total} | 27.4 m |

The height of the stratified corium pool was computed using the core inventory data [31] of BWR-5 – fifth generation reactor of the GE’s BWR family. The coefficient R used to calculate the corium layer volumes of the quasi-SMR was based on the ratio of thermal powers:

$$R = \frac{P_t(BWRX - 300)}{P_t(BWR - 5)} \quad (2.1)$$

Table 2.3: Properties of oxidic and metallic layers

| Parameter | BWR-5 | Quasi-SMR |
|---------------------------------|----------------------|----------------------|
| Power (thermal) P_t | 2029 MW _t | 870 MW _t |
| Coefficient R | 0.43 | |
| Oxide layer volume V_{ox} | 10.07 m ³ | 4.330 m ³ |
| Metallic layer volume V_{met} | 2.43 m ³ | 1.045 m ³ |

Based on the key parameters of the RPV and the calculated volumes of the oxide and the metal layer, layer heights can be computed.

$$H_i = \frac{V_i}{\pi R^2} = \frac{4V_i}{\pi D^2} \quad (2.2)$$

Table 2.4: Stratified corium pool layer heights

| | |
|---|---------|
| Oxide layer height H_{ox} | 0.345 m |
| Metallic layer height H_{met} | 0.083 m |

Based on the obtained layer heights, geometry of the stratified lower plenum of the quasi-SMR was modelled. Since no detailed design documents of the BWRX-300 were available, the lower head was simplified. During the IVMR operation, the whole volume of the containment structure would not be flooded. To consider this, the water level was

set to 1 meter from the bottom. Part of the RPV in contact with air above the water is not modelled because based on the different heat transfer coefficients of air and water the heat exchange between the RPV and air would be negligible. Disregarding the upper part of the RPV also saves a lot of computational resource as the corium pool situates only in the lower 2% of the RPV.

As discussed in 2.1.1, 2D axisymmetric domain is chosen to model the flow domain. This means disregarding the CRGTs as for BWR-type reactors, control rods enter from below (Figure 2.2).

To obtain the axisymmetric 2D geometry, the 3D domain with the axis on the X-axis and the whole domain above the local $Y=0$ plane must be modelled. Therefore, the first step is to model a quarter sector of the 3D model and then badge the 2D parts to obtain the 2D geometry (Figure 2.3).

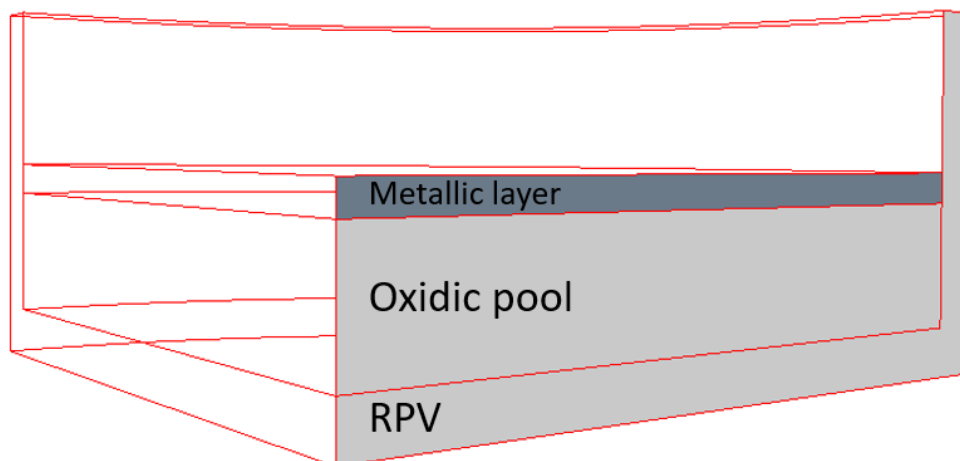


Figure 2.3: Quarter sector of the 3D model with badged 2D parts

2.2 Boundary and initial conditions

The next step of the CFD analysis process (Table 2.1) is to establish boundary and initial conditions. Each obtained part (metallic layer, oxidic pool, RPV) is assigned to a region and their initial and boundary conditions are given. This ensures the simulation to start from an initial solution and to use an iterative method to reach a final flow field steady-state solution. [23]

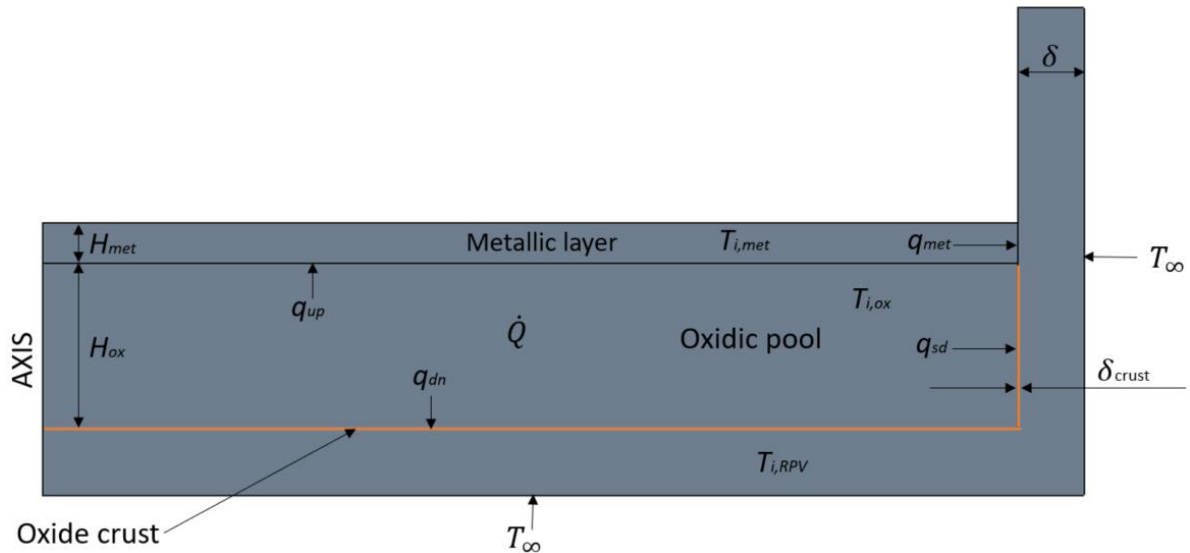


Figure 2.4: Graphical representation of parameters

2.2.1 Reactor pressure vessel

The material used for reactor pressure vessel is SA-508 [30]. The needed properties of the alloy are shown in Table 2.5. The values are constant.

Table 2.5: Thermal properties of the RPV [32]

| Property | Value |
|--------------------------------|------------------------|
| Density ρ_{RPV} | 7600 kg/m ³ |
| Specific heat $C_{p,RPV}$ | 625 J/kg · K |
| Thermal conductivity k_{RPV} | 35 W/m · K |

The initial temperature $T_{i,RPV}$ of the RPV is set to 25°C. The outer side and bottom boundary of the RPV would be surrounded by water at T_{∞} , which is set to static temperature of 100°C.

The top section of the RPV, which is not modelled, affects the heat exchange minimally so the boundary between the bottom and the top section (upper boundary of the modelled RPV region) is assumed to be adiabatic. If anything, these assumptions contribute to the conservativeness of the analysis.

2.2.2 Oxidic pool

The oxidic pool consists of UO_2 and ZrO_2 . The height of the oxidic pool H_{ox} is previously obtained in Table 2.4. The mass composition of the layer is based on the reduced size of BWR-5 [31]. The necessary thermal properties of the layer are shown in Table 2.6.

Table 2.6: Properties of oxidic and metallic layers [31]

| Property | Notation (unit) | Oxidic pool | Metallic layer |
|-------------------------------|--------------------------|-------------|----------------|
| Thermal expansion coefficient | β (1/K) | 1.05E-04 | 1.10E-04 |
| Thermal conductivity | k ($W/m \cdot K$) | 5.3 | 31.4 |
| Dynamic viscosity | μ ($Pa \cdot s$) | 5.35E-03 | 4.00E-03 |
| Specific heat | C_p ($J/kg \cdot K$) | 508.10 | 539.53 |
| Density | ρ (kg/m^3) | 8467.85 | 6302.82 |
| Liquidus temperature | T_i (K) | 2973 | 1600 |

The initial temperature of the oxidic pool is set to the liquidus temperature of the oxidic layer at 2973 K. All boundaries are conducting whereas between the oxidic pool and the RPV there is conjugate heat transfer and between oxidic and metallic layers there is a conducting baffle.

Oxide crust

Due to the melting and solidification processes in the oxidic domain, the so-called corium crust is formed at the periphery of the oxidic pool. This is a key phenomenon for the IVMR strategy as due to the lower thermal conductivity of the crust, the focusing effect in the metallic layer takes place. The crust acts as a thermal and mass transfer resistance at different layer configurations, establishing the pool formations.

The current model takes the oxidic crust into account as a stationary model without any physical domain. The effect of the crust is modeled by thermal insulance, which is a function of thermal conductivity and thickness of the crust:

$$R_{\lambda,crust} = \frac{\delta_{crust}}{k_{crust}}, \quad (2.3)$$

where k_{crust} is the thermal conductivity and δ_{crust} is the thickness of the oxidic crust. Based on the crust's thermal conductivity value from [2] and the approximate constant thickness of the crust at 1 cm, the thermal insulance of the crust is

$$R_{\lambda,crust} = \frac{\delta_{crust}}{k_{crust}} = \frac{0.01}{3.73} = 0.00268 \frac{\text{m}^2 \cdot \text{K}}{\text{W}}, \quad (2.4)$$

The approximate thickness of the crust is obtained by monitoring the temperature field during the simulation and assessing the average thickness of the sub-liquidus temperature layer at the boundary.

The crust's insulation is modelled only at the oxide-RPV interface since the temperatures between the oxidic and metallic layers are higher than the liquidus temperature of the oxidic crust which would melt the crust at the oxidic-metallic layer interface.

Volumetric heat source

The heat generation rate is assumed to be distributed in the oxidic pool since the main component of the layer is UO_2 which holds the decay heat from the fission process. To set a uniform value throughout the domain, volumetric heat source option is used in the oxidic pool.

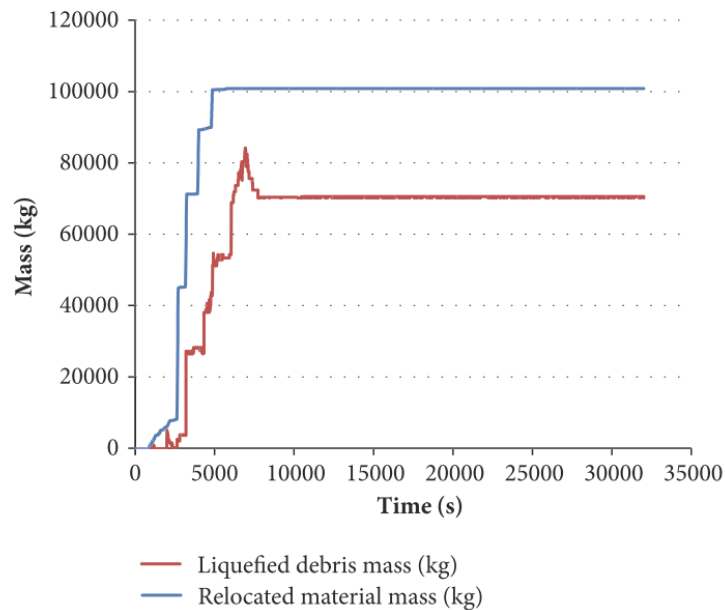


Figure 2.5: Liquefied and relocated debris mass of BWR-5 [31]

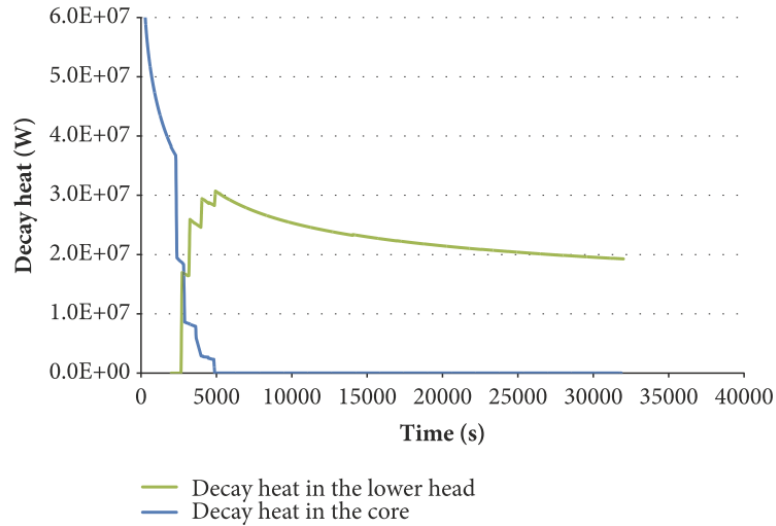


Figure 2.6: Decay heat in the reactor core and the lower head of BWR-5 [31]

Two main parameters that define the total residual (decay) heat are the volume of the oxidic pool and the timing for the two-layered configuration [2]. As seen in Figure 2.5, the whole liquefaction takes place after ~ 7500 seconds. In Figure 2.6, the corresponding decay heat for BWR-5 at $t = 7500$ seconds would be ~ 27 MW. Multiplying the result with the coefficient R from Table 2.3, the total residual heat of the quasi-SMR would be 11.6 MW.

To obtain the volumetric heat source value, the residual heat must be divided by the volume of the domain:

$$\dot{Q} = \frac{Q}{V} = \frac{11.6}{4.33} = 2.68 \frac{\text{MW}}{\text{m}^3} \quad (2.5)$$

This value is extremely conservative as it does not consider the time for stratification nor the lower initial residual power of the SMR which would cause the debris to liquefy and relocate slower than the 7500 seconds assumed in the present case. Longer time to relocate would therefore lead to lower decay heat and lower volumetric heat source value. The conservativity is also displayed when comparing the 7500 second timing with the assessed timing of 4+ hours (14400+ seconds) of AP-600 [2]. In the latter case, the total residual heat in the lower head of the quasi-SMR would be ~ 10 MW and the volumetric heat source therefore ~ 2.3 MW/m³.

2.2.3 Metallic layer

The height of the metallic layer H_{met} is previously obtained in Table 2.4. The mass composition of the layer is based on the reduced size of BWR-5 [31]. The necessary thermal properties of the layer are shown in Table 2.6.

The initial temperature of the metallic layer is set to the liquidus temperature of the oxidic layer as the two-layered configuration is formed by stratification which means active heat transfer and the convergence of the temperatures in the whole lower plenum.

As mentioned before, the oxidic-metallic layer interface acts as a conducting baffle interface; the metallic layer-RPV interface as conjugate heat transfer wall and the top boundary of the metallic layer is adiabatic to maximize the conservativity of the model.

2.3 Mesh generation

To simulate the flow, the domain is discretized into a grid. STAR-CCM+ has a built-in automated mesher which generates surface and volume meshes for its input parts. The mesh generator decomposes the flow domain into control volumes [33].

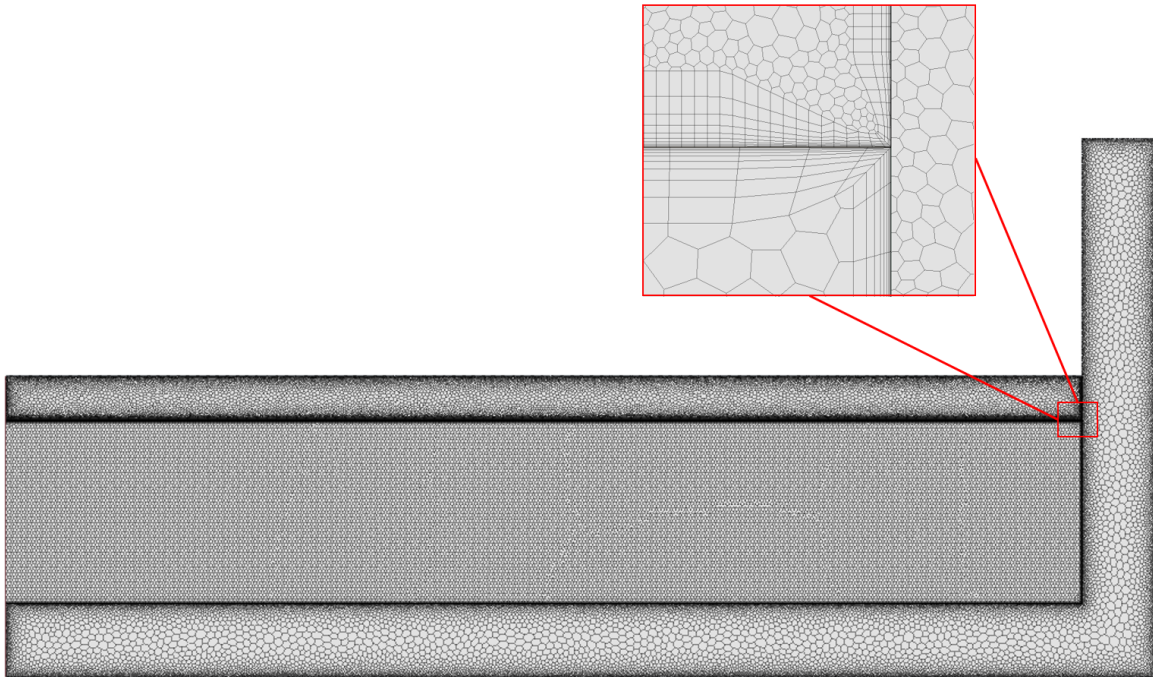


Figure 2.7: Generated mesh of the simulation domain

The mesh must consider among other things the velocity profile, the phase of the medium, computational resource, and the curvature of the domain. In this work's case, the velocity and its gradient are the highest along the walls as the hotter and lighter fluid cools down and becomes denser.

Regarding the velocity profile along the wall in the fluid, the boundary layers have to be resolved thoroughly in order to accurately simulate the mass flow and heat exchange at the boundary. A layer of structured prismatic cells is used to capture the strong transverse gradients of the solution with less numerical diffusion than an unstructured volume mesh would. As velocity field is present only in the fluid domain, prism cells are not necessary at solid regions (Figure 2.7).

When generating the prism layer, the most important boundary layer parameter to monitor is the y^+ value. y^+ is interpretable as a local Reynolds number that determines

the relative importance of viscous and turbulent processes. The wall region is divided into layers depending on the y^+ value. The layers are:

1. The viscous sublayer ($y^+ < 5$) – the fluid is dominated by the viscous effect and the Reynolds shear stress is negligible
2. The logarithmic area ($y^+ > 30$) – turbulence stress dominates the flow and velocity profile varies slowly along the distance y
3. The buffer layer ($5 < y^+ < 30$) – the buffer layer is the transition between the viscous sublayer and the logarithmic area. Viscous and turbulent stresses are of similar magnitude

A suitable y^+ value is defined by the choice of turbulence model and is subject to optimization through remeshing. The current model uses Low Reynolds Standard K-Epsilon (Low-Re SKE) model, which for the higher accuracy in natural convection cases should have a $y^+ \leq 1$. To achieve a satisfactory y^+ value, the height of the first layer of prism cells can be adjusted while keeping the total layer and stretch factor (a ratio of neighbouring layer heights) within required limits. The y^+ value for the mesh was well below 1 for all wall regions to leave a margin for the greater cell size in the mesh independence study step of the CFD analysis process.

To account for varying meshing considerations in different regions, all three regions are meshed separately. For all regions, the bulk of the region is meshed using polygonal mesher and for metallic and oxidic layers, prism layer mesher is used at the boundaries (Figure 2.7). The total cell count of all regions is displayed in Table 2.7.

Table 2.7: Cell count of the regions in the used mesh

| Part | Cell count |
|----------------|-------------------|
| RPV | 47 371 |
| Oxidic layer | 30 512 |
| Metallic layer | 23 222 |
| TOTAL | 101 105 |

The growth rate of the cells in the oxidic layer is as low as possible (~ 1) because of the volumetric heat source in the layer. Through trial and error, the layer demonstrated bad convergence per heat balance if the growth rate was not close to 1.

2.4 Simulation strategy

Simulation strategy involves determining things as the use of the turbulence model, melting and solidification model, the choice of the solver etc. After deciding on the strategy, the simulation has to be validated against a reliable experiment in the field to assess the error the model produces.

Due to the turbulent nature of the natural convection heat transfer in the melt core, the correct choice of the turbulent model is necessary. This can be achieved by simulating a corresponding experiment and comparing the errors of different turbulence models to find the most appropriate one. Due to the two-dimensional geometry of the model, the large eddy simulation models (LES) are not able to resolve the turbulence. Therefore, the Reynolds-averaged Navier-Stokes (RANS) based models are used to model the turbulence in the domain.

Several CFD studies have shown that the numerical simulations for the flow configurations associated with the core melt scenarios are challenging. By validation study, Aounallah et al [34] concluded that the $k-\omega$ SST model provided more accurate results than the $k-\epsilon$ model. However, the models have always had difficulties reproducing the mean flow [35].

The Algebraic heat flux model by Nuclear Research and Consultancy Group (AHFM-NRG+) was developed in 2018 to provide better results for natural, mixed, and forced convection flow regimes for unity and low Prandtl fluids. The model is based on Low-Reynolds Standard $k-\epsilon$ turbulent model which is in turn calibrated by changing the coefficients (Table 2.8) of the Temperature Flux Model in STAR-CCM+. [35]

Table 2.8: Temperature Flux Model coefficients of AHFM-NRG+

| Model coefficient | Value |
|-------------------|--|
| R | 0.5 |
| Sigma-Theta2 | 1 |
| Ctu0 | 0.2 |
| Ctu1 | 0.25 |
| Ctu3 | $-4.5 \cdot 10^{-9} \cdot \log^7(Ra \cdot Pr) + 2.5$ |
| Ctu4 | 0 |

The coefficient $Ctu3$ has a significant influence on the prediction of natural convection flows, and it highly depends on the Rayleigh and Prandtl number values of the corresponding domain. Therefore, a logarithmic function of the values of Ra and Pr define the value of the coefficient. Thanks to this correlative coefficient, the model can be efficiently used for different working fluids.

Due to the difference in Rayleigh and Prandtl numbers, the coefficients differ for the metal and oxide layer. The calculated values of the $Ctu3$ coefficients for both stratified layers are shown in Table 2.9.

Table 2.9: $Ctu3$ coefficient calculations for different layers

| Layer | Rayleigh number | Prandtl number | $Ctu3$ coefficient |
|----------|----------------------|----------------|--------------------|
| OXIDIC | $3.04 \cdot 10^{12}$ | 0.5129 | 2.32 |
| METALLIC | $1.79 \cdot 10^6$ | 0.0687 | 2.5 |

Furthermore, a constant density model together with the Boussinesq approximation is used. Boussinesq approximation ignores any changes in the fluid density due to temperature gradients except in the weight term in the momentum equation. Boussinesq model can be used for flows with small temperature differences. The density variations are assumed to have a linear dependence on temperature: [36]

$$\rho = \rho_0 - \beta \rho_0 (T - T_0) \quad (2.11)$$

The turbulent Prandtl number (Pr_t) is necessary to solve the heat transfer problem of two-dimensional turbulent boundary layer flows. Modelling in this work employs a constant turbulent Prandtl number of 0.9 – a default value set in STAR-CCM+.

2.4.1 Validation against BALI experiment

BALI experiment was designed in 1993 to create a knowledge basis about heat transfer distribution at boundaries of corium pools for in-vessel or ex-vessel configurations. The BALI facility uses water as simulant fluid for corium whereas the same magnitude for Prandtl number is maintained as for oxidic corium. Volumetric heating of the domain is achieved by direct current heating in a 2D full scale 15cm thick hemi-cylindrical geometry (Figure 2.8). The facility is externally cooled by a coolant which causes the water in the domain to solidify. [11]

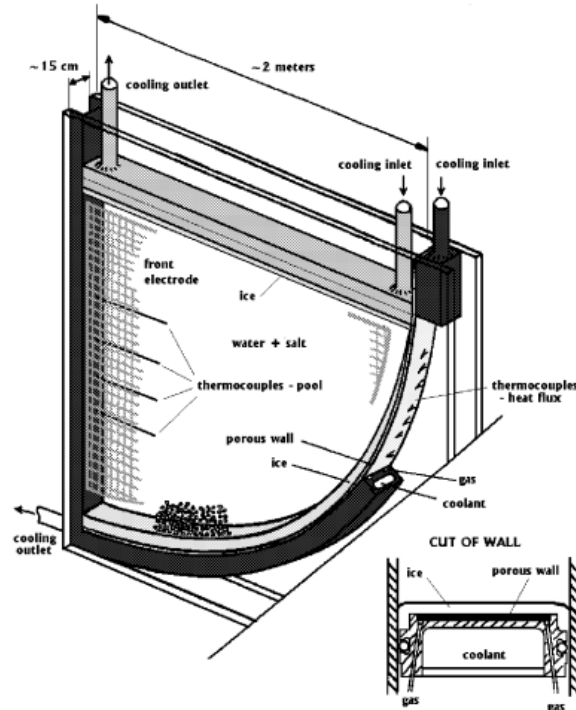


Figure 2.8: BALI in-vessel test section

To compare the experimental results to the results from the simulation, 5 parameters are monitored using the same physics models as in the main IVMR simulation:

1. Internal Rayleigh number Ra_i
2. External Rayleigh number Ra_e
3. Nusselt number of the top section Nu_{top}
4. Nusselt number of the curved section Nu_{cv}
5. Ratio Q_{curved}/Q

All of the solver and model settings are the same as mentioned before apart from the Ctu3 coefficient. The Ctu3 coefficient used in the BALI case is 0.5.

In addition to validating the physics models, the choice between segregated and coupled flow solvers is made based on the error and total CPU solver time. Even though coupled solvers are usually recommended in the natural convection case, segregated fluid solvers are easier to use and the AHFM-NRG+ turbulence model was validated using a segregated fluid solver together with the segregated fluid temperature model. [35]

In order to account for the ice formation, the bottom part of the geometry is cut which simplifies the problem because ice formation can therefore be set as a boundary

condition. Every wall except the left one has the boundary condition of constant temperature of 273K. The boundary condition of the left vertical wall is adiabatic.

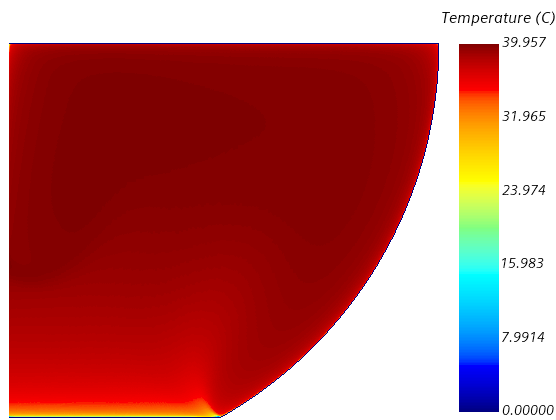


Figure 2.9: Temperature field of the BALI simulation

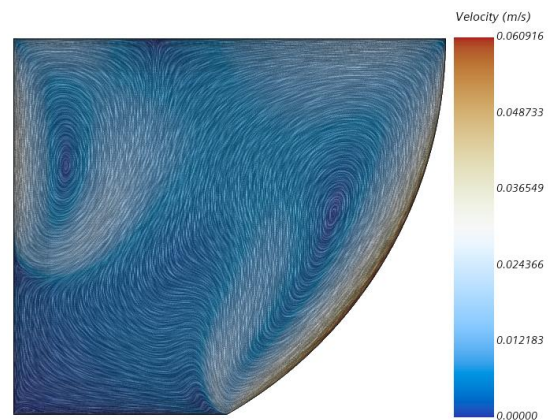


Figure 2.10. Velocity field of the BALI simulation

The mesh used to simulate the BALI experiment consists of 200K cells. The main volume is meshed by polygonal mesher and the walls are meshed using a prism layer mesher. There are 10 prism layers at each wall expect the adiabatic vertical wall.

To shorten the time necessary until the absolute convergence, an iterative convergence error of 1% is allowed. Convergence is measured by monitoring the heat balance and the mean temperature fluctuations. An iterative convergence error of 1% in this case means that the results are gathered when the temperature is not visibly rising and

$$Q_{out} = 0.99 \cdot Q_{in} \quad (2.12)$$

where Q_{out} is the heat going out through the top, bottom and the curved part of the wall and Q_{in} is the volumetric heat source which in this simulation's case is 15.7 kW.

Table 2.10: Results of the validation

| | Experiment | Coupled | Segregated | Coupled error | Segregated error |
|----------------------------|------------|----------|------------|---------------|------------------|
| Ra_internal | 2.27E+16 | 2.64E+16 | 2.66E+16 | 16% | 17% |
| Ra_external | 3.75E+12 | 4.58E+12 | 4.43E+12 | 22% | 18% |
| Nu_top | 2693 | 2397.6 | 2468.44 | 11% | 8% |
| Nu_curved | 1441 | 1614.6 | 1642.85 | 12% | 14% |
| Q_curved/Q | 0.524 | 0.4 | 0.39 | 24% | 26% |
| Solver CPU time [s] | | 100556 | 33894 | | |

Figures 2.9 and 2.10 present the temperature and velocity fields of the validated BALI experiment. The results of the validation (Table 2.10) show how accurately the AHFM-NRG+ turbulence model solves the BALI experiment problem compared to the other turbulence models used in [35]. Considering the iterative convergence error of 1%, the results are satisfactory. In comparison, coupled solver is less accurate than the segregated solver while being computationally ~ 3 times more demanding. Hence the segregated flow solver would be used to simulate the main IVMR strategy problem.

2.5 Mesh Independence Study

The simulation process has to be repeated to examine sensitivities of the computed results and the computational efficiency. Verification assessment process consists of multiple steps, one of them being the mesh independence study. Examining grid convergence is necessary to determine the ordered discretization error in the simulation. The method involves performing the simulation on successively finer grids. [37]

A grid convergence index GCI provides consistent way of reporting the results of grid convergence. The GCI can be computed using two levels of grid but three are recommended to accurately estimate the convergence. GCI also provides a result based on Richardson's extrapolation as the grid resolution approaches zero. The GCI shows how much the solution would change with a further grid refinement. The GCI is defined as: [37]

$$GCI = F_s \cdot \frac{|\epsilon|}{r^p - 1} \quad (2.13)$$

where F_s is a factor of safety, ϵ is the relative error compared to the finer grid, r is the grid refinement ratio, p is the order of convergence. When comparing three or more grids, the factor of safety is $F_s = 1.25$. The grid refinement ratio r can be computed from:

$$r = \left(\frac{N_1}{N_2}\right)^{\frac{1}{D}} \quad (2.14)$$

where N is the total number of grid points used for the grid and D is the dimension of the flow domain. The order of convergence p can be obtained from three solutions of the three grids:

$$p = \ln\left(\frac{f_3 - f_2}{f_2 - f_1}\right) / \ln(r) \quad (2.15)$$

where f is the solution of the grid.

After finding the grid convergence indices for 3 grids, the solutions have to be checked to be in the asymptotic range of convergence for the computed solution:

$$GCI_{23} = r^p GCI_{12} \quad (2.16)$$

2.5.1 Grid convergence study of the IVMR problem

To determine the ordered discretization error and the result as the grid resolution approaches zero, a grid convergence study is carried out with the solutions of the simulations of varying grid resolutions. The most important parameter regarding the IVMR strategy is the external heat flux of the RPV. Therefore, this maximum local heat flux would be the monitored. As all of the regions are meshed separately, the effects of different combinations are too great to alter the mesh size of each region. Hence, only the mesh size of the oxidic pool is changed due to the volumetric heat source in the layer.

Table 2.11: Grid convergence study input data

| Case no | Base size (mm) | Cell count | RPV max flux (W/m^2) |
|---------|----------------|------------|--------------------------|
| 1 | 8,66 | 47040 | 748347,37 |
| 2 | 11 | 30512 | 747615,55 |
| 3 | 15 | 18472 | 746424,48 |

Based on the input from Table 2.11 we can examine the grid convergence of the simulation. The grid refinement ratio r is found for both grid refinement operations 1-2 and 2-3. The order of convergence is then found based on the average value of both grid refinement ratios. Solutions are indeed in the asymptotic range of convergence as the R value is approximately 1. Finally, through Richardson extrapolation, the assumption for obtaining the maximum local heat flux at zero grid spacing can be made.

Table 2.12: Grid convergence study results

| | r | p | error | GCI | R | flux h=0 |
|------------------|----------|-----------|-----------|--------|-------------|-----------|
| Grids 1-2 | 1.241648 | 2.0829237 | 0.0009779 | 0.195% | 1.000978881 | 749513.59 |
| Grids 2-3 | 1.285223 | | 0.0015932 | 0.317% | | |
| AVG | 1.263435 | | | | | |

The grid convergence study results are shown in Table 2.12. Based on the grid convergence study, the maximum local heat flux is estimated to be 749 514 W/m^2 with an error band of 0.195% or 0.002.

2.6 Simulation results

The final step of the CFD analysis process encompasses post-processing the simulation and documenting the findings of the analysis.

The temperature field of the complete model (Figure 2.11) visualizes the potential creep and ablation/melting region that would occur in the RPV due to the higher than melting temperatures. The melting point of SA-508 steel is 1500°C [32]. The line between the grey and blue are in Figure 2. represents the melting temperature of the steel. It has to be noted that due to the melting and addition of steel, the focusing effect and the thermal load would decrease.

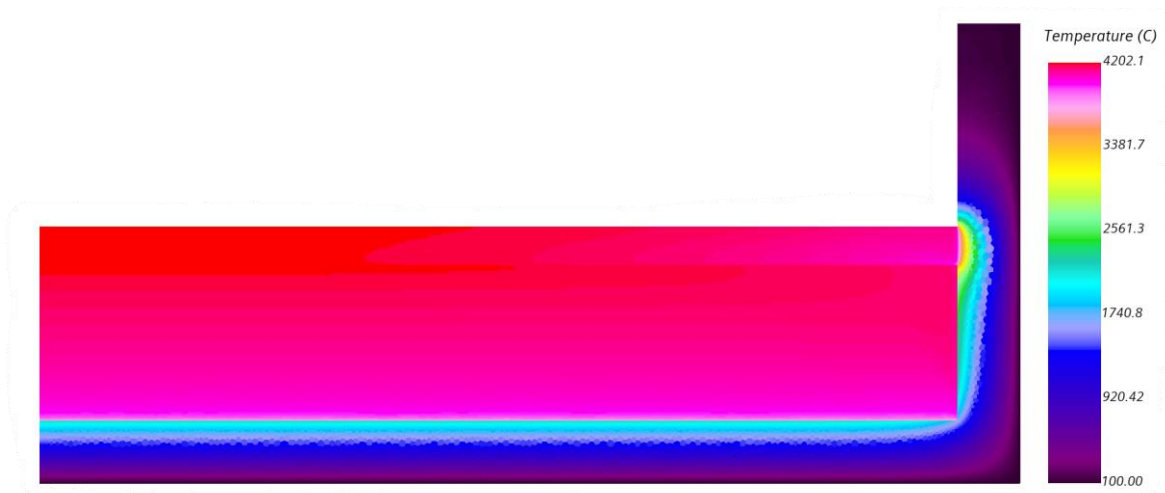


Figure 2.11: Temperature field of the complete model

More specifically, the temperature field in the fluid regions (Figure 2.12) shows, how the highest temperature area is by the radial axis in the metallic layer. The average temperature of the metallic layer is 4150°C and 4112°C for the oxidic pool. The actual temperature would be lower due to radiative heat flux off the top layer of the metallic pool.

The temperature field of the fluid regions shows the lack of temperature areas under the liquidus temperature of the oxidic pool which would mean that there would be no crust present. The crust would in fact appear in the region of the RPV creep due to the differences of liquidus temperature of the oxide crust and the melting point of the RPV.

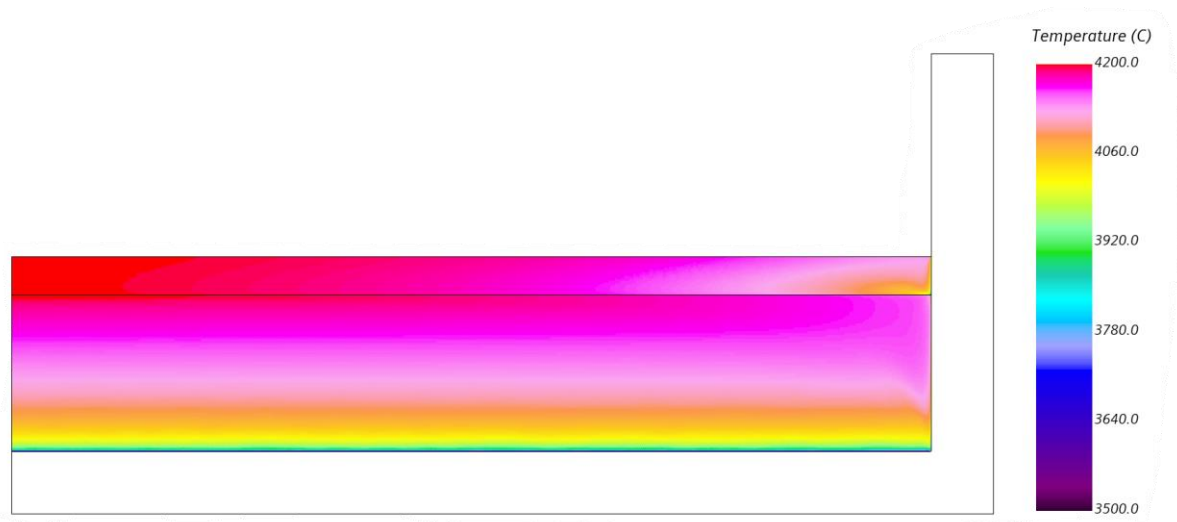


Figure 2.12: Temperature field of the fluid regions

The velocity field of the fluid regions (Figure 2.13) demonstrates the natural convective nature of the flow. As fluids cool by the walls, they become denser, and the flow path is formed. From Figure 2.12 and Figure 2.13 it is visible how the internal stratification patterns in the oxidic pool are formed.

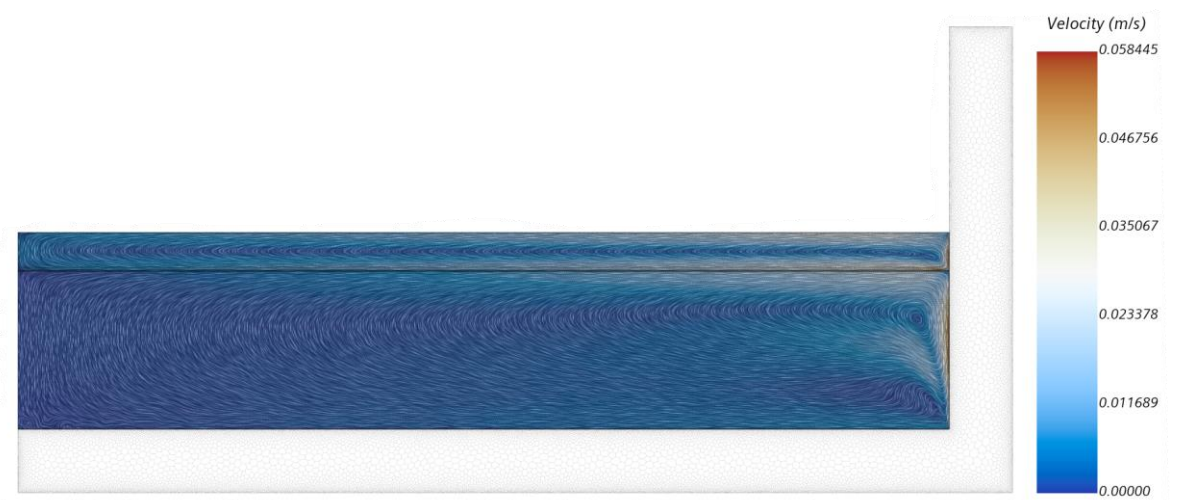


Figure 2.13: Velocity field of the fluid regions

The local boundary heat flux of the outer wall of RPV is shown in Figure 2.14. This demonstrates the focusing effect in action as the highest local heat flux is at the location of the metallic layer. The downward heat flux is $\sim 0.5 \text{ MW/m}^2$ and it is uniform as the thickness of the corium crust is constant. The side-wall heat flux presents the impact of the focusing effect as the local heat flux is at maximum at the metal layer's height. The maximum local heat flux based on the simulation and the grid convergence study is $\sim 0.75 \text{ MW/m}^2$.



Figure 2.14: Outer heat flux profile of the RPV

The maximum local heat flux value stays comfortably well below the CHF value of $\sim 1.5 \text{ MW/m}^2$ [2] (computed from 1.15) which corresponds to the CHF value at $\theta = 0^\circ$. The most dangerous situation, however, is in the transient phase due to different layer configurations of the corium pool. The maximum heat fluxes in the transient phases show an increase of 1.6-2.4 times compared to steady-state simulation [38]. This would mean maximum heat fluxes up to 1.8 MW/m^2 , which would already cause a boiling crisis.

3. CONCLUSIONS AND DISCUSSION

The current knowledge makes it possible to adopt the IVMR strategy to conventional reactors that are at or below 600 MWe. For SMRs, the compact design poses series of challenges which makes the re-assessment of the strategy necessary before adoption for these types of designs.

As a result of the simulation, the maximum local heat flux in steady-state configuration in case of 11.6 MW decay heat was found out to be $\sim 0.75 \text{ MW/m}^2$, which is well below the CHF but could present problems in the transient situations. The maximum heat fluxes in transient phases could be up to 2.4 times higher which would already cause a boiling crisis.

The results of the simulation are consistent based on the BALI experiment and comparing the velocity and temperature profiles of other studies. However, the temperatures of both metallic and oxidic layers are significantly higher than mentioned in the literature. This could be caused by too conservative decay heat value.

The most influential parameter to define the maximum local heat flux is the value of the volumetric heat source. Therefore, as the assumed decay heat is conservative, the result also is conservative. The accuracy of the model could greatly be improved by calculating the decay heat more precisely using appropriate codes. Because decay heat depends on the timing of the accident, implementation of suitable codes would be needed to simulate the melting process as well.

The model could also be greatly improved by implementing melting and solidification physics models of the corium pool and the RPV. This would simulate the real conditions more accurately and highlight the actual magnitude of the creep more precisely. This would be the next necessary step to implement in order to highlight the coolant's ability to maintain the structural integrity of the RPV.

The IVMR strategy itself could be upgraded by implementing number of engineering practices, the most notable ones being in-vessel injection and external coating of the vessel. Injection would greatly decrease the concentration factor, therefore diminishing the negative consequences of the focusing effect during the transient phases. External coating has been proven to work in small-scale experiments, but they have to be tested in bigger scale in order to become a feasible part of the IVMR strategy.

SUMMARY

Nuclear energy has been a low-emission energy source for over 60 years. During this time, there have been three major accidents which have also resulted in the nuclear core overheating and relocating. The corium continues to emit decay heat which raises the temperature of the pool and the reactor pressure vessel (RPV).

The molten corium could either be let to penetrate the reactor pressure vessel and caught by an external core-catcher or it could be kept inside the reactor pressure vessel by externally cooling the vessel. The latter strategy is called In-vessel melt retention (IVMR) strategy and it has been proven to work for sub-600 MWe LWRs such as VVER-400 and AP-600. Due to geometrical limitations of small modular reactors, the IVMR strategy should be re-assessed. This thesis acts as a preliminary estimation for the feasibility of the strategy for SMRs.

The applicability of the IVMR strategy depends on the heat transfer between the reactor pressure vessel and the surrounding cooling agent to preserve the structural integrity of the RPV. The most cost-effective and abundant coolant is water which is also considered for the IVMR strategy.

The heat transfer between the RPV and the surrounding water is complex due to the boiling and bubble formation at the RPV-water boundary. As the heat flux from the vessel rises, a dangerous phenomenon – boiling crisis - could present itself. The boiling crisis occurs when the heat flux from the RPV exceeds the critical heat flux (CHF) of water at set conditions.

The magnitude of the heat flux from the corium pool to the RPV and the consequent flux from RPV to surrounding water depends on the stratification of the pool. As the fuel assemblies and the internal structures melt due to the temperature rise, the pool starts to stratify because of density differences. The pool undergoes several configurations until it reaches a two-layered steady state with oxidic pool in the bottom and metallic layer on top. The oxidic layer has a high liquidus temperature which results in the crust formation at the pool-RPV interface. This in turn causes the upward heat flux from the oxidic pool to the metallic layer to increase.

The amplification of heat flux on the RPV wall is described by focusing effect which depends on the height of the metallic layer, the radius of the corium pool, the heat flux from the oxidic pool, and the boundary conditions. The focusing effect decreases with the increase of the metallic layer height which is why the most dangerous configurations

are the transient ones where the metallic layer has not fully developed, and the decay heat is higher than in the steady state.

The second part of the thesis focuses on the numerical modelling of the quasi-SMR to assess the thermal hydraulic phenomena and the maximum local heat flux from the RPV to the surrounding water. The CFD analysis was performed using STAR-CCM+ to model the lower head of the reactor pressure vessel and the stratified two-layered corium pool.

The geometry was built up using 2D axial symmetry, whereas the parameters of the RPV were obtained from BWRX-300 and the ones of the corium pool from reduced BWR-5. The oxide crust was modelled as thermal insulation and the decay heat was distributed in the oxidic pool as volumetric heat source. The turbulent model used in the simulation was AHFM-NRG+ which is based on the Low-Reynolds Standard K-Epsilon turbulence model in conjunction with the temperature flux model. The density fluctuations were modelled by using Boussinesq model.

The numerical model was validated against the BALI experiment which was developed in 1999 to investigate the melt pool convection and heat transfer. The validation results were satisfactory and presented similar results with the experiment. As part of the validation, segregated flow solver was selected due to higher computational efficiency compared to coupled flow solver.

After the validation, the model was applied to the 2D axisymmetric geometry of the quasi-SMR. The velocity and temperature fields presented similar flow patterns as confirmed by the previous works. As a result of the simulation, the maximum local heat flux in steady-state configuration in case of 11.6 MW decay heat was found out to be $\sim 0.75 \text{ MW/m}^2$, which is well below the CHF but could present problems in the transient situations.

KOKKUVÕTE

Tuumaenergia on olnud inimkonna jaoks madalaheitmelise elektri allikas üle 60 aasta. Selle aja sees on toimunud kolm suuremat õnnetust, mille tagajärjel on toimunud reaktori tuuma sulamine ja selle ümberpaigutumine. Sulaolekus kooriumis jätkub jääksoojuse teke, mille tagajärjel suureneb kooriumi ja surveanuma temperatuur.

Sulanud kooriumiga on võimalik käituda kahel viisil - sellel võib lasta sulada läbi reaktori surveanuma ning seejärel püüda see spetsiaalse tuumapüüdjaga või hoida sulanud massi reaktori surveanuma sees välise jahutuse abil. Teist strateegiat nimetatakse IVMR (*In-vessel melt retention*) strateegiaks. Arvutuslikult ning eksperimentaalselt on tõestatud IVMR strateegia sobivus alla 600 MWe kergveereaktoritele nagu näiteks VVER-400 ja AP-600. Väikeste moodulreaktorite (VMR) geomeetriliste ja disainiliste iseärasuste tõttu tuleb üle vaadata IVMR sobivus VMRide puhul. See lõputöö esitab esialgse hinnangu IVMR strateegia sobivusest VMRidele.

IVMR strateegia rakendatavus sõltub soojusvahetustest reaktori surveanuma ja ümbritseva jahutusagensi vahel, et säilitada surveanuma struktuuriline terviklikkus. Kõige ökonoomsem ja laialdaselt kasutatavam jahutusvedelik on vesi, mis on kesksel kohal ka IVMR strateegia puhul.

Soojusvahetus surveanuma ja ümbritseva vee vahel on keeruline erinevate keemismehhanismide ja mullide tekkimise tõttu surveanuma ja vee piirpinnal. Soojusvoo suurenemine võib kaasa tuua keemise kriisi – ohtliku fenomeni, mis esineb juhul, kui surveanumast pärinev soojusvoog ületab kriitilise soojuskoormuse ja mullkeemine läheb üle kelmeliseks keemiseks.

Soojuskoormuse väärtus kooriumi ja surveanuma ning surveanuma ja ümbritseva vee vahel sõltub kooriumi kihistumisest. Sulanud kütusekoostude ja sisemiste terasstruktuuride tiheduste erinevuste tõttu on kooriumil iseloomulikud kihistumismustrid. Lõplikus tasakaaluseisundis on koorium kahes kihis – all olev oksiidikiht ning pealne sulametallikiht. Oksiidikihil on kõrge sulamistemperatuur, mistõttu moodustub oksiidikihi ja surveanuma piirile oksiidikoorik. Kooriku moodustumine suurendab kahe kihi vahelist soojuskoormust.

Soojusvoo võimendumist surveanuma seinal kirjeldab koondumiseefekt, mis sõltub metallikihi kõrgusest, surveanuma sisemisest raadiusest, oksiidikihi soojusvoost ning ääritingimustest. Koondumiseefekt väheneb metallikihi kõrguse suurenemisega, mistõttu on kõige ohtlikumad kihistumiskonfiguratsioonid sellised, kus pealne

metallikiht on õhukene. Vastavad ohuolukorrad on just üleminekufaasid, kui metallikiht pole täielikult välja arenenud ning jääksoojus on kõrgem kui tasakaaluolekus.

Lõputöö teine osa keskendub väikese moodulreaktori numbrilisele modelleerimisele, et hinnata termohüdraulilisi fenomene ning maksimaalset soojuskoormust reaktori surveanuma ja ümbritseva vee vahel. CFD (*Computational Fluid Dynamics*) analüüs on läbi viidud kasutades STAR-CCM+ tarkvara. Selleks on modelleeritud reaktori surveanuma alumine osa ning kahekihiline koorium.

Mudeli geomeetria on kujutatud 2D aksisümmeetrilisena, kusjuures surveanuma parameetrid pärinevad BWRX-300 andmetest ning kooriumi parameetrid vähendatud BWR-5 andmetest. Oksiidikoorig on modelleeritud soojusisolatsioonina ning jääksoojus on ühtlaselt jaotunud oksiidikihis. Turbulentsimudelina on kasutusel AHFM-NRG+, mis põhineb Low-Reynolds Standard K-Epsilon mudelil ja temperatuuri voo mudelil. Tiheduse muutumine on modelleeritud kasutades Boussinesqi lähendust.

Kasutatav STAR-CCM+ mudel on valideeritud kasutades BALI eksperimenti, mis viidi läbi 1999. aastal, et uurida kooriumi konvektsiooni ja soojusvahetust. Valideerimise tulemused olid rahuldavad ja tulemused sarnanesid eksperimentaalsetele tulemustele. Lisaks tulemuste hindamisele osutus edasiste arvutuste tegemiseks valituks eraldatud lahendaja kasutamine, kuna see pakkus võrreldes sidestatud lahendajaga oluliselt suuremat arvutusökonoomsust.

Pärast valideerimist rakendati füüsikamudel eelmainitud 2D aksisümmeetrilisele geomeetria. Simulatsiooni tulemusel väljajoonistunud kiirus- ja temperatuuriväljad sarnanesid varasemate tööde omadega. 11,6 MW jääksoojuse korral on maksimaalne soojuskoormus tasakaaluolekus $\sim 0,75 \text{ MW/m}^2$, mis jääb küll alla kriitilise soojuskoormuse, kuid mis võib tekitada probleeme üleminekufaasides.

Maksimaalset soojuskoormust mõjutab kõige rohkem valitud jääksoojuse väärtus. Kuna töös kasutatud jääksoojus on konservatiivne, siis on ka saadud tulemus konservatiivne. Mudelit saab oluliselt arendada rakendades sulamis- ja tahkestumismudelid kooriumile ja reaktori surveanumale, mille abil saaks täpsemalt simuleerida oksiidikoorigu teket ja selle mõju ning surveanuma sulamisulatust.

LIST OF REFERENCES

- [1] M. M. Gospodarczyk and M. Nari Fisher, 'IAEA Releases 2019 Data on Nuclear Power Plants Operating Experience', *IAEA Department of Nuclear Energy*, 2020. <https://www.iaea.org/newscenter/news/iaea-releases-2019-data-on-nuclear-power-plants-operating-experience> (accessed Jun. 01, 2021).
- [2] T. G. Theofanous, C. Liu, S. Additon, S. Angelini, O. Kymäläinen, and T. Salmassi, 'In-vessel coolability and retention of a core melt', *Nucl. Eng. Des.*, vol. 169, no. 1-3, pp. 1-48, 1997, doi: 10.1016/S0029-5493(97)00009-5.
- [3] R. E. Henry and H. K. Fauske, 'External cooling of a reactor vessel under severe accident conditions', *Nucl. Eng. Des.*, vol. 139, no. 1, pp. 31-43, Jan. 1993, doi: 10.1016/0029-5493(93)90260-G.
- [4] O. Kymäläinen, H. Tuomisto, and T. G. Theofanous, 'In-vessel retention of corium at the Loviisa plant', *Nucl. Eng. Des.*, vol. 169, no. 1-3, pp. 109-130, Jun. 1997, doi: 10.1016/s0029-5493(96)01280-0.
- [5] F. Fichot, J.-M. Bonnet, and B. Chaumont, 'IRSN views and perspectives on in-vessel melt retention strategy for severe accident mitigation', *EUROSAFE Forum*, p. 15, 2015, [Online]. Available: https://www.researchgate.net/profile/Florian_Fichot/publication/291295233_IRSN_views_and_perspectives_on_in-vessel_melt_retention_strategy_for_severe_accident_mitigation/links/569f502208ae21a56425af58/IRSN-views-and-perspectives-on-in-vessel-melt-retentio.
- [6] L. Carénini, F. Fichot, and B. P. St, 'Analysis of critical points of the In-Vessel Retention safety evaluation', pp. 1-10, 2020.
- [7] A. Ots, *Soojustehnika aluskursus: Termodünaamika. Põlemine. Soojusülekanne*. Tallinn: TTÜ Kirjastus, 2011.
- [8] Y. Li, 'CFD Pre-test Analysis of SIMECO-2 Experiment', no. July, 2016.
- [9] L. Carénini and F. Fichot, 'The impact of transient behavior of corium in the lower head of a reactor vessel for in-vessel melt retention strategies', in *International Conference on Nuclear Engineering, Proceedings, ICONE*, Oct. 2016, vol. 4, doi: 10.1115/ICONE24-60598.
- [10] R. Le Tellier, L. Saas, and S. Bajard, 'Transient stratification modelling of a corium

- pool in a LWR vessel lower head', *Nucl. Eng. Des.*, vol. 287, pp. 68–77, Jun. 2015, doi: 10.1016/j.nucengdes.2015.02.009.
- [11] J. M. Bonnet, 'Thermal hydraulic phenomena in corium pools: the BALI experiment'. 1999, Accessed: Mar. 23, 2021. [Online]. Available: http://inis.iaea.org/Search/search.aspx?orig_q=RN:30061089.
- [12] C. T. Tran, P. Kudinov, and T. N. Dinh, 'An approach to numerical simulation and analysis of molten corium coolability in a boiling water reactor lower head', in *Nuclear Engineering and Design*, Sep. 2010, vol. 240, no. 9, pp. 2148–2159, doi: 10.1016/j.nucengdes.2009.11.029.
- [13] L. Viot, R. Le Tellier, and M. Peybernes, 'Modeling of the corium crust of a stratified corium pool during severe accidents in light water reactors', *Nucl. Eng. Des.*, vol. 368, p. 110816, Nov. 2020, doi: 10.1016/j.nucengdes.2020.110816.
- [14] L. Carénini, F. Fichot, and N. Seignour, 'Modelling issues related to molten pool behaviour in case of In-Vessel Retention strategy', *Ann. Nucl. Energy*, vol. 118, pp. 363–374, 2018, doi: 10.1016/j.anucene.2018.04.032.
- [15] Nuclear Power, 'Decay Heat - Decay Energy', 2021. <https://www.nuclear-power.net/nuclear-power/reactor-physics/reactor-operation/residual-heat/decay-heat-decay-energy/> (accessed Jun. 02, 2021).
- [16] N. Touran, 'Decay heat: Why you can't just turn off nuclear reactors', *WhatIsNuclear*. <https://whatisnuclear.com/decay-heat.html> (accessed May 18, 2021).
- [17] B. J. Ade and I. C. Gauld, 'Decay Heat Calculations for PWR and BWR Assemblies Fueled with Uranium and Plutonium Mixed Oxide Fuel Using Scale', 2011. Accessed: Jun. 02, 2021. [Online]. Available: <http://www.osti.gov/contact.html>.
- [18] S. Globe and D. Dropkin, 'Natural-Convection Heat Transfer in Liquids Confined by Two Horizontal Plates and Heated From Below', *J. Heat Transfer*, vol. 81, no. 1, pp. 24–28, Feb. 1959, doi: 10.1115/1.4008124.
- [19] S. W. Churchill and H. H. S. Chu, 'Correlating equations for laminar and turbulent free convection from a vertical plate', *Int. J. Heat Mass Transf.*, vol. 18, no. 11, pp. 1323–1329, Nov. 1975, doi: 10.1016/0017-9310(75)90243-4.
- [20] X. Wang and X. Cheng, 'Analysis of focusing effect of light metallic layer in stratified molten pool under IVR-ERVC condition', *J. Nucl. Eng. Radiat. Sci.*, vol.

- 1, no. 2, Apr. 2015, doi: 10.1115/1.4029619.
- [21] C. E. Brennen, *Thermo-Hydraulics of Nuclear Reactors*. Cambridge University Press, 2016.
- [22] F. Fichot *et al.*, 'Some considerations to improve the methodology to assess In-Vessel Retention strategy for high-power reactors', *Ann. Nucl. Energy*, vol. 119, pp. 36–45, 2018, doi: 10.1016/j.anucene.2018.03.040.
- [23] The NPARC Alliance, 'CFD Analysis Process', 2021. <https://www.grc.nasa.gov/www/wind/valid/tutorial/process.html>.
- [24] Siemens Digital Industries Software, 'Simcenter STAR-CCM+', 2021. <https://www.plm.automation.siemens.com/global/en/products/simcenter/STAR-CCM.html>.
- [25] Imperial College London, 'Spinout companies', 2021. <https://www.imperial.ac.uk/mechanical-engineering/about-us/spinout-companies/> (accessed May 07, 2021).
- [26] S. H. Kim, H. K. Park, and B. J. Chung, 'Two- and three-dimensional experiments for oxide pool in in-vessel retention of core melts', *Nucl. Eng. Technol.*, vol. 49, no. 7, pp. 1405–1413, Oct. 2017, doi: 10.1016/j.net.2017.05.008.
- [27] C. Torregrosa, W. Villanueva, C. T. Tran, and P. Kudinov, 'Coupled 3D thermo-mechanical analysis of a nordic BWR vessel failure and timing', *Proc. 15th Int. Top. Meet. Nucl. React. Therm. Hydraul.*, no. September 2015, 2013.
- [28] J. W. Bae and B. J. Chung, 'Comparisons of 2-D and 3-D IVR experiments for oxide layer in the three-layer configuration', *Nucl. Eng. Technol.*, vol. 52, no. 11, pp. 2499–2510, Nov. 2020, doi: 10.1016/j.net.2020.04.016.
- [29] A. Filippov and D. Kamenskay, 'CFD SIMULATIONS OF MELT-VESSEL INTERACTION IN CONTEXT OF IVMR PROBLEM', 2019.
- [30] GE-Hitachi Nuclear Energy, 'BWRX-300 General Description', no. July, 2020.
- [31] M. Valinčius, T. Kaliatka, A. Kaliatka, and E. Ušpuras, 'Modelling of Severe Accident and In-Vessel Melt Retention Possibilities in BWR Type Reactor', *Sci. Technol. Nucl. Install.*, vol. 2018, 2018, doi: 10.1155/2018/7162387.
- [32] J. Jung, S. M. An, K. S. Ha, and H. Y. Kim, 'Evaluation of heat-flux distribution at

the inner and outer reactor vessel walls under the in-vessel retention through external reactor vessel cooling condition', *Nucl. Eng. Technol.*, vol. 47, no. 1, pp. 66–73, 2015, doi: 10.1016/j.net.2014.11.005.

- [33] ManchesterCFD team, 'All there is to know about different mesh types in CFD!', *University of Manchester*. <https://www.manchestercfd.co.uk/post/all-there-is-to-know-about-different-mesh-types-in-cfd> (accessed May 11, 2021).
- [34] M. Aounallah, Y. Addad, S. Benhamadouche, O. Imine, L. Adjlout, and D. Laurence, 'Numerical investigation of turbulent natural convection in an inclined square cavity with a hot wavy wall', *Int. J. Heat Mass Transf.*, vol. 50, no. 9–10, pp. 1683–1693, May 2007, doi: 10.1016/j.ijheatmasstransfer.2006.10.015.
- [35] A. Shams, 'Towards the accurate numerical prediction of thermal hydraulic phenomena in corium pools', *Ann. Nucl. Energy*, vol. 117, no. 2018, pp. 234–246, 2018, doi: 10.1016/j.anucene.2018.03.031.
- [36] Siemens PLM Software, 'STAR-CCM+ User Manual'. <https://docs.sw.siemens.com/documentation/external/PL20201113103827399/en-US/userManual/userguide/html/index.html> (accessed May 12, 2021).
- [37] The NPARC Alliance, 'Examining Spatial (Grid) Convergence', 2021. <https://www.grc.nasa.gov/www/wind/valid/tutorial/spatconv.html> (accessed May 13, 2021).
- [38] L. Carénini *et al.*, 'Main outcomes from the IVR code benchmark performed in the European IVMR project', *Ann. Nucl. Energy*, vol. 146, p. 107612, Oct. 2020, doi: 10.1016/j.anucene.2020.107612.

APPENDIX 1 Pikendatud kokkuvõte

Tuumaenergia on olnud elektrivõrgu osa aastast 1954, kui Nõukogude Liidus Obniskis ühendati võrku 5 MW jaam. Alates sellest ajast on inimkonnal üle 18 000 reaktoriaasta kogemust. Selle aja jooksul on toimunud kolm suuremat õnnetust, mis on ka viinud osalise või täieliku tuuma ülessulamiseni – olukorrani, mis esineb, kui reaktori poolt toodetud energia ületab jahutusvedeliku poolt ärajuhitava soojuse. Selle tagajärjel soojus akumuleerub kütusekoostudes ja temperatuuri tõusu tagajärjel need hakkavad sulama. Sulanud tuumkütuse ja terasstruktuuride mass – koorium – paigutub ümber reaktori surveanuma põhja.

Sulanud kooriumiga on võimalik käituda kahel viisil - sellel võib lasta sulada läbi reaktori surveanuma ning seejärel püüda see spetsiaalse tuumapüüdjaga või hoida sulanud massi reaktori surveanuma sees välise jahutuse abil. Teist strateegiat nimetatakse IVMR (*In-vessel melt retention*) strateegiaks. Arvutuslikult ning eksperimentaalselt on tõestatud IVMR strateegia sobivus alla 600 MWe kergveereaktoritele nagu näiteks VVER-400 ja AP-600. Väikeste moodulreaktorite (VMR) geomeetriliste ja disainiliste iseärasuste tõttu tuleb üle vaadata IVMR sobivus VMRide puhul.

Selle lõputöö eesmärk on kirjeldada kihistunud kooriumi termohüdraulilisi fenomene ning anda esialgse hinnang IVMR strateegia sobivusest VMRidele. Selleks on läbi viidud CFD (*Computational Fluid Dynamics*) analüüs Simcenter STAR-CCM+ tarkvaraga. Lõputöö esimene osa keskendub IVMR strateegia teoreetilistele alustele ja teine osa kirjeldab modelleerimis- ja simulatsiooniprotsessi.

A1.1 IVMR strateegia

IVMR strateegia töötati välja pärast Three Mile Islandi tuumaõnnetust, kui üheks võimalikuks ohuolukorrana pidi arvestama, et vee täielikku aurustumist ja seeläbi vahetatut jahutust pole võimalik tagada. Hoidmaks kooriumi siiski reaktori surveanumas, pakuti lahenduseks välja surveanuma väline jahutamine selle uputamise veete.

IVMR strateegia on atraktiivne, kuna selle abil hoitakse suurt hulka radioaktiivset massi koos erituvate gaasidega reaktori surveanumas, kus on seda lihtsam monitoorida. Kõige robustsemal viisil on IVMR strateegia ka odavam, kui välise tuumapüüdja paigaldamine.

IVMR strateegia on robustne ja lihtne, kuna selle aktiveerimiseks on vaja ainult kaht tegevust – kaitsekesta täitmine veega ja seeläbi reaktori surveanuma alumise osa vette

sukeldamine ning surveanuma rõhu alt vabastamine. IVMR strateegia suurimateks takistusteks on kooriumi keeruline uuritavus ning seeläbi tekkivad küsitavused. Eksperimentaalselt ei ole võimalik täielikus suuruses vastavaid fenomene kujutada, mistõttu on vajalik teha palju eeldusi, mis ei pruugi täielikult vastata tegelikkusele.

Strateegia on siiani atraktiivne, kuid rakendatavus on uute reaktorite kõrge võimsuse tõttu piiratud. Kuigi VMRid on kuni 300 MWe võimsusega, siis nende integraalne disain loob uued väljakutsed IVMR strateegia kasutuselevõtuks. Seetõttu on vajalik hinnata IVMR strateegia pädevust ka VMRide puhul.

A1.1.1 Kooriumi termohüdraulika

Ümberpaigutatunud kooriumis on põhilised liikumapanevad jõud seletatavad vabakonvektsiooni fenomenidega, mida saab kirjeldada sarnasusarvudega – Grashof (Gr), Prandtl (Pr) ja Damköhler (Da). Termohüdraulika sõltub suuresti ka Rayleigh numbri väärtusest, mis on sisemise soojusallikaga vedelikele defineeritud kui (1.1). Rayleigh number ilma soojusallikata vedelikele on defineeritud kui (1.2).

Grashofi arv (1.3) iseloomustab vabakonvektsiooniga seotud soojuslevi – see kirjeldab vedelikule mõjuvat temperatuuride vahest tingitud jõudu.

Prandtl arv (1.4) kirjeldab hüdrodünaamilise ja termilise piirkihi paksuse vahet. Mida suurem on Prandtl arvu väärtus, seda paksem on hüdrodünaamiline piirkiht võrreldes termilise piirkihiga. Prandtl arv on vedeliku füüsikaline omadus ja ei sõltu geomeetristest mõõtmetest, mistõttu on see tihti toodud ka tabelites välja.

Damköhleri arv (1.5) kirjeldab reaktsiooni ja konvektsiooni ajaskaalade suhet ning sellega seotakse IVMR strateegia puhul soojuse generatsioon selle ülekandumise kiirusega.

Sõltuva sarnasusarvuna kasutatav Nusselti arv (1.6) näitab soojusülekanne teguri ja keskkonna soojusjuhtivusteguri suhet. Nusselti arv kirjeldab soojusülekanne vedeliku ja tahke keha piirpinnal. Kui Nusselti väärtus on umbes 1, siis konvektsioon ja konduktsioon on sarnase suurusjärguga. Suurem Nusselti arv tähistab aktiivsemat konvektsiooni ja seetõttu kirjeldab turbulentsset voolamist.

Kihistumisprotsess

Koorium koosneb neljast põhilisest komponendist – tsirkooniumist, terasest, uraanist ja hapnikust. Sulanud U-Zr-O-Fe mass kihistub vastavalt komponentide oksüdeerumisele ja tiheduste erinevusele oksiidikihtiks ja metallikihtiks.

Pärast esmast tuumakoostude sulamist tekib surveanuma põhja raske metalli kiht, mis hakkab edasisel terasstruktuuride lisandumisel tõusma pinnale, liikudes seejuures läbi oksiidikihi ja tekitades kolmekihilise konfiguratsiooni ja lõpuks kahekihilise tasakaaluseisundi, kus metallikiht on oksiidikihi peal. Kihistumise kiiruse suurimaks määramatuseks on difusioonikoefitsiendi väärtus ja selle mõju, kuna puuduvad eksperimentaalsed allikad.

Oksiidikiht

Oksiidikihi kõige tähtsam näitaja on Nusselti arv, kuna see kirjeldab soojusvahetust metallikihi ja seeläbi koondumise efekti suurusjärku ja selle mõju. Üldine oksiidikihti soojusbilanss avaldub kujul (1.8). Kuna kahekihilise konfiguratsiooni korral on oksiidikiht põhjas, siis peab silmas pidama ka erinevate reaktoritüüpide erinevaid geometriaid. Keevveereaktorite puhul sisenevad kontrollvardad surveanuma alt, mistõttu on voolused erinevad, kui Joonisel 1.2, kus on võimalik selgelt eristada piirikihi regiooni, hästi segunenud ülemist kihti ning kihistunud alumist osa.

Oksiidikihi kõrge sulamistemperatuuri tõttu moodustub oksiidikihi ja surveanuma piirile koorik, mida iseloomustab madal soojusjuhtivustegur ning muutuv paksus. Oksiidikoarik on üks võtmetegureid IVMR strateegia rakendamisel. Koorik tekib algselt ka metallikihi ja oksiidikihi vahele, kuid metallikihi temperatuuri tõusmisel see sulab ning koorik jääb ainult surveanuma piirpinnale.

Soojuse teke on IVMR strateegia puhul määratud lihtsuse huvides oksiidikihti. Soojus tekib oksiidikihis jääsoojuse tõttu, mis langeb küll pärast tavaoperatsiooni lõppu koheselt ~7% täisvõimsusest (Figure 1.4), kuid sellegi poolest kujutab akumulatsioon suurt ohtu. Jääsoojuse suurust hinnates tuleb arvesse võtta aega, mis kulub tavaoperatsiooni lõpust kuni kahekihilise tasakaaluseisundi tekkimiseni. Kalkulatsioonide konservatiivsuse huvides peaks eeldama minimaalset võimalikku aega. AP-600 reaktori puhul on vastavaks ajaks hinnatud 4+ tundi.

Metallikiht

Metallikiht koosneb rauast (Fe) ja tsirkooniumist (Zr), mis on omavahel segunenud. Jääsoojus oksiidikihist jaguneb kaheks – üks osa kandub konduktsioonina välja horisontaalselt läbi surveanuma seina ja teine osa lahkeb metallikihist läbi pealmise piirpinna soojuskiirgusena. Metallikihi soojusbilanss avaldub seega kujul (1.11).

IVMR strateegia puhul on üheks oluliseks näitajaks metallikihis tekkiv koondumise efekt, mida kirjeldab kontsentratsioonifaktor (1.12), mis tähistab väljuva vertikaalse soojusvoo ja oksiidikihist siseneva soojusvoo suhet. Kuna metallikihist väljuv soojuslik

kiirgus on võrreldes teiste voogudega tühine, siis muutub koondumise efekt suuremaks ja üldine käsitlus konservatiivsemaks. Avaldada on aga kontsentratsioonifaktorit lihtsam, kuna see taandub surveanuma raadiuse ja metallikihi kõrguse suhte võrdelisuseks (1.13).

Kontsentratsioonifaktor väheneb metallikihi kõrguse ja surveanuma raadiuse suhte suurenemisega. See tähendab, et kontsentratsioonifaktorit ja koondumise efekti mõjutab eelkõige metallikihi kõrgus, mistõttu on kõige ohtlikumad olukorrad just üleminekufaasid, kui metallikiht on alles välja kujunemas.

A1.1.2 Surveanuma purunemine

Surveanuma purunemise kriitilisim mehhanism on keemise kriisi teke, mis seisneb mullkeemise üleminekus kelmeliseks keemiseks. Kelmeline keemine toob kaasa oluliselt halvema soojusülekanne, kuna piirpind on kaetud aurukelmega, mille soojusülekanne on oluliselt madalam kui vedeliku oma.

Punkt, mille juures tekib keemise kriis, kannab nime kriitiline soojuskoormus. Kriitiline soojuskoormus on suurim kooriumi horisontaalsel teljel, kus leiab aset ka selles töös uuritav koondumise efekt. Kriitiline soojuskoormus ei ole konstantne väärtus, vaid sõltub erinevatest teguritest keemise keeruliste mehhanismide tõttu. Sellegi poolest on robustselt võimalik hinnata surveanuma ümber toimuva keemise kriitilist soojuskoormust vastavalt (1.15).

Surveanuma purunemine saab toimuda vaid keemise kriisi korral, mistõttu on keemise kriisi teke eelduseks surveanuma purunemisele.

A1.1.3 IVMR strateegia tõhususe tõstmine

Kuigi IVMR strateegia on küllaltki robustne, on võimalik selle tõhusust tõsta innovaatilisi meetodeid kasutades, mis vajaksid rakendamiseks veel edaspidist teadus- ja arendustööd.

Terase hulga tõstmine reaktorituumas vähendaks koondumise efekti ulatust, kuna selle tulemusel pakseneks pealmine metallikiht ja seega väheneks kontsentratsioonifaktor. Teras kogust saab tõsta lisades tuuma terasstruktuure, mis sulades suurendaksid kooriumi terase hulka ning samas ka eemaldaksid süsteemist soojust struktuuride sulades.

Üleminekufaaside efektide vähendamiseks on üheks võimaluseks ka surveanumasisene jahutus läbi pritsimise, mille tagajärjel jahtuks kooriumi pealmine kiht ning seeläbi

lisanduks pealmine jahutus. Samuti suurendaks see Zr oksüdatsiooni, mis avaldaks mõju kooriumi kihistumisele.

Surveanuma väline katmine kattekihiga suurendaks kriitilise soojuskoormuse väärtust kuni 25%. Vastavad väikesemõõtmelised eksperimendid vajaksid veel täiendavat uurimist, et neid rakendada täissuuruses reaktoritel.

Surveanuma jahutamise täiustamine seisneb lisaks vabakonvektsioonile ka sundkonvektsiooni kasutamises, et soojusvahetus surveanuma ning ümbritseva vee vahel oleks efektiivsem. Kuigi see tõstaks soojusvahetuse tõhusust, suurendaks see ohutussüsteemi aktiivsust, mis ei oleks uusimate trendidega kooskõlas. Lisaks võib suurendada IVMR strateegia efektiivsust ka surveanuma väline pritsimine kuni väline veekiht ei ole saavutanud oma lõplikku kõrgust, et aeglustada tuuma sulamisprotsessi.

A1.2 Kooriumi modelleerimine

Lõputöö teine osa kirjeldab kooriumi ja seda ümbritseva reaktori surveanuma modelleerimist ja tasakaaluseisundi simuleerimist. Simulatsioon on läbi viidud kaubanduslikult saadaval oleva tarkvaraga Simcenter STAR-CCM+, mis kuulub Siemens Digital Industries Software tarkvaraportfelli. STAR-CCM+ on CFD tarkvara, mis võimaldab simuleerida erinevaid vooluseid ja olukordi. Integreeritud keskkonnas on võimalik luua geomeetria, võrku, voolusimulatsioone ja põhjalikku järeلتöötlust.

A1.2.1 Mõõtmeliskus ja geomeetria

IVMR strateegia ja kooriumi termohüdraulika uurimise eesmärgil on läbi viidud arvukalt eksperimente nii 2D kui ka 3D anumates. Tegelikuses toimub protsess muidugi 3D keskkonnas, kuid simulatsiooni silmas pidades on 3D arvutuslikult palju nõudlikum, mistõttu piisava täpsuse korral oleks oluliselt ökonoomsem kasutada 2D geomeetria.

Võrreldes 3D geomeetriaga on 2D voolused ühel pinnal. See toob 3D geomeetria puhul vertikaalsete vooluste hajumise radiaalselt ning seeläbi nende nõrgenemise. Selle tulemusel väheneb vertikaalne soojusvahetus. Kuna 2D voolused on lineaarsed, siis ülessuunatud soojusvahetus on ühtlasem ning tugevam. Lisaks on eksperimentide tulemusel märgatud ka koondumise efekti väiksemat mõju 3D geomeetria puhul.

Keevaveereaktorite (BWR – *Boiling water reactor*) puhul peab silmas pidama, et kontrollvardad sisenevad reaktorituuma ning surveanumasse alt, mistõttu ei looks aksisümmeetriline 2D modelleerimine õiget pilti BWRi tegelikust geomeetriast. Kuna aga

kontrollvarraste ümber on lokaalne jahutus, siis tegelikkuses vähendavad kontrollvarraste juhttorud kooriumi temperatuuri.

Võttes arvesse BWR-tüüpi reaktorite eripärasid ning 2D ja 3D geomeetria mõju voolusele ning soojusvahetusele, on mõistlik viia simulatsioon läbi aksisümmeetrilise 2D geomeetriaga, kuna see on konservatiivne ning arvutuslikult kordades tõhusam kui 3D geomeetria.

Surveanuma geomeetria mõõtmeks on kasutatud GE-Hitachi BWRX-300 VMRi mõõtmeid. BWRX-300 on 300 MWe keevaveereaktor, mis on 10. generatsiooni keevaveereaktor GE BWR-ide nimistust. Modelleerimiseks olulised parameetrid on toodud Tabelis 2.2.

Kihistunud kooriumi kõrgus on arvatud võttes arvesse BWR-5 reaktori tuuma koostist ning soojuslikku võimsust. Leidmaks vastavaid kihtide kõrguseid VMR-tüüpi reaktorile, on vastavad kõrgused läbi korrutatud koefitsiendiga R (2.1), mis on võrdne BWRX-300 ja BWR-5 soojuslike võimsuste suhtega. Kooriumi kihtide ruumalad ja kõrgused on toodud Tabelites 2.3 ja 2.4.

Surveanuma ja kooriumi täielikul modelleerimisel on märgata, et surveanuma kõrgus on palju kõrgem kui põhja koguneva kooriumi kõrgus. Seetõttu on arvutuslikku efektiivsust silmas pidades mõistlik eirata surveanuma ülemist osa. Lõpliku domeenina on arvestatud ainult alumist 1 m surveanumast.

A1.2.2 Ääre- ja algingimused

Surveanuma materjal on SA-508 teras ning materjali vastavad soojuslikud omadused on toodud Tabelis 2.5. Surveanuma välimised ääred on konstantsel temperatuuril 100°C , mis tähistab vee keemistemperatuuri. Surveanuma ülemine äärelõige on adiabaatiline.

Oksiidikihi füüsikalised omadused on toodud Tabelis 2.6. Oksiidikihi algtemperatuuriks on seatud sulamistemperatuur 2973 K . Oksiidikoorig on modelleeritud soojusisolatsioonina, kusjuures arvestatud paksus on konstantne. Oksiidikoorig puudub metalli- ja oksiidikihi vahel, kuna temperatuuride tõusmisel koorik sulaks.

Soojuse teke jääsoojusena on seatud ainult oksiidikihti. Konservatiivselt on arvestatud, et tuuma ümberpaigutumine toimub ~ 7500 sekundiga, mis hetkel on soojusliku võimsuse väärtus $\sim 11.6\text{ MW}$. See aeg ei arvesta kihistumiseks kuluvat aega ega ka VMRi väiksemat soojuslikku võimsust, mille tagajärjel toimuksid sulamisprotsessid aeglasemalt.

Metallikihi füüsikalised omadused on toodud Tabelis 2.6. Metallikihi algtemperatuuriks on seatud oksiidikihi sulamistemperatuur, kuna kihistumise tulemusena on temperatuurid ühtlustunud.

Vooluse simuleerimiseks tuleb domeen diskretiseerida võrguks. Võtmaks arvesse erinevaid vooluprofiile ning materjale, on kõik kolm regiooni diskretiseeritud eraldi. Näiteks oksiidikihi võrgu puhul tuleb luua võimalikult ühtlane võrk, kuna sisemise soojuse tekke tõttu võivad muul juhul esineda simulatsiooni konvergeerumises vead.

A1.2.3 Simulatsiooni strateegia

Kooriumis toimuvad termohüdraulilised voolused on turbulentsed, mistõttu on üheks kõige tähtsamaks osaks täpse simulatsiooni loomisel õige turbulentsimudeli valimine. Käesolevas lõputöös on kasutatud AHFM-NRG+ mudelit, mis põhineb *Low Reynolds Standard K-Epsilon* (Low-Re SKE) turbulentsimudelil. Low-Re SKE on lisaks kalibreeritud STAR-CCM+ sisseehitatud *Temperature Flux Model* koefitsientide muutmise abil. Vastavad koefitsiendid on toodud Tabelis 2.8 ja 2.9.

Turbulentsimudeli pädevuse hindamiseks on läbi viidud ka valideerimine BALI eksperimendiga. BALI eksperiment viidi läbi 1999. aastal, et uurida kooriumi konvektsiooni ja soojusvahetust. Valideerimise tulemused olid rahuldavad ja tulemused sarnanesid eksperimentaalsetele tulemustele. Lisaks tulemuste hindamisele osutus edasiste arvutuste tegemiseks valituks eraldatud lahendaja kasutamine, kuna see pakkus võrreldes sidestatud lahendajaga oluliselt suuremat arvutusökonoomsust. Valideerimise tulemused on toodud Tabelis 2.10.

Lisaks läbi viidud võrgu sõltumatuse uuring on vajalik, et hinnata diskretiseerimisest tingitud vea suurust ning hinnata simulatsiooni tulemust lõpmatu tiheda võrgu korral. Uuringu tulemusena selgus, et võrk on koonduv.

A1.2.4 Simulatsiooni tulemused

Temperatuuri- ja kiirusvälja joonistelt (Joonised 2.11 – 2.13) joonistuvad välja ligikaudne terase sulamise ulatus, kõrgtemperatuursed alad ning vabakonvektsioonile iseloomulikud voolused. Jooniselt 2.14 on näha surveanuma soojuskoormuse välja. See piltlikustab koondumise efekti ning oksiidikooriku mõju. Simulatsiooni ja võrgu sõltumatuse uuringu tulemusena on maksimaalne kohalik soojuskoormus ~ 0.75 MW/m², mis jääks alla kriitilise soojuskoormuse, kuid kujutaks keemise kriisi tekkeohtu üleminekufaasides, kus soojuskoormus võib olla kuni 2,4 korda tasakaaluseisundi väärtusest.